

Coarse-grained models for fluids and their mixtures: Comparison of Monte Carlo studies of their phase behavior with perturbation theory and experiment

B. M. Mognetti^(a), P. Virnau, L. Yelash, W. Paul, K. Binder

Institut für Physik, Johannes Gutenberg Universität Mainz,

Staudinger Weg 7, 55099 Mainz, Germany

M. Müller

Institut für Theoretische Physik, Georg-August-Universität Göttingen

Friedrich-Hund-Platz 1, 37077 Göttingen, Germany

and

L. G. MacDowell

Dpto de Química Física, Facultad de Cc. Químicas,

Universidad Complutense, 28040 Madrid, Spain

The prediction of the equation of state and the phase behavior of simple fluids (noble gases, carbon dioxide, benzene, methane, short alkane chains) and their mixtures by Monte Carlo computer simulation and analytic approximations based on thermodynamic perturbation theory is discussed. Molecules are described by coarse grained (CG) models, where either the whole molecule (carbon dioxide, benzene, methane) or a group of a few successive CH_2 groups (in the case of alkanes) are lumped into an effective point particle. Interactions among these point particles are fitted by Lennard-Jones (LJ) potentials such that the vapor-liquid critical point of the fluid is reproduced in agreement with experiment; in the case of quadrupolar molecules a quadrupole-quadrupole interaction is included. These models are shown to provide a satisfactory description of the liquid-vapour phase diagram of these pure fluids. Investigations of mixtures, using the Lorentz-Berthelot (LB) combining rule, also produce satisfactory results if compared with experiment, while in some previous attempts (in which polar solvents were modelled without explicitly taking into account quadrupolar interaction), strong violations of the LB rules were required. For this reason, the present investigation is a step towards predictive

modelling of polar mixtures at low computational cost. In many cases Monte Carlo simulations of such models (employing the grand-canonical ensemble together with reweighting techniques, successive umbrella sampling, and finite size scaling) yield accurate results in very good agreement with experimental data. Simulation results are quantitatively compared to an analytical approximation for the equation of state of the same model, which is computationally much more efficient, and some systematic discrepancies are discussed. These very simple coarse-grained models of small molecules developed here should be useful e.g. for simulations of polymer solutions with such molecules as solvent.

PACS numbers: 05.70.Ce, 64.70.F-, 64.75.Cd, 02.70.Tt a) Electronic mail: mognetti@uni-mainz.de

I. INTRODUCTION

It has been a longstanding challenge to predict accurately the equation of state and in particular the phase diagrams of fluids and fluid mixtures from atomistic models via computer simulation.^{1,2,3,4,5} Such applications have required a widespread development of computer simulation methodology: significant advances were possible through the invention of Gibbs ensemble^{6,7,8} and configurational bias^{9,10,11} methodologies, grand canonical Monte Carlo simulations combined with histogram reweighting methods^{12,13,14} and finite size scaling^{15,16,17,18} including field mixing,^{19,20,21,22} umbrella sampling^{23,24} and other expanded ensemble methods.^{25,26,27} A lot of effort has also been spent towards developing more and more accurate effective potentials from quantum chemistry methods (e.g. Refs. 28,29,30,31,32,33). However, for simple and industrially relevant fluids such as carbon dioxide^{34,35} it is still difficult to predict the equation of state with high accuracy, such that experimental data in the critical region and for temperatures $\pm 30\%$ around it are reproduced to an accuracy of a few percent.^{36,37} Extending such calculations to mixtures (in particular, solutions of polymers with supercritical carbon dioxide as a solvent) is even more of a problem, due to the less complete knowledge of effective potentials, and due to the extensive numerical effort required. A three-dimensional parameter space involving the variables temperature T , pressure p and mole fraction x needs to be scanned for a binary system,

and the phase diagrams are typically very complicated, because vapor-liquid and fluid-fluid phase equilibria compete with each other.^{38,39,40,41} If polymers are chosen as a solute, their molecular weight enters as an additional fourth variable. Moreover, the coarse-grained representation of the solvent (e.g. carbon dioxide) and the solute have to be compatible, i.e., one cannot combine an atomistic description of the solvent with a much coarser representation of a macromolecular solute. There is clearly a need to devise models that are simple enough to allow extensive simulation studies with an affordable effort and nevertheless accurate enough to be interesting for applications to experiment and in the context of industrial processing. Such validated coarse-grained models that accurately reproduce thermodynamic bulk properties are also a starting point for investigating the kinetics of phase separation or spatially inhomogeneous systems (e.g. wetting and catalysis).

In the present work, we wish to make a step towards this goal, extending our previous study of a selected sample of simple pure fluids, in particular carbon dioxide^{36,37} to various binary mixtures. We want to stress that our aim is not to reach the most accurate prediction of the phase diagram of a specific system. Indeed, motivated by the excellent results obtained for the pure carbon dioxide and for simple quadrupolar molecules in general,³⁶ we want to investigate how this model performs for mixtures, especially solutions of various alkanes. In particular we will show that the new coarse grained (CG) model avoids the need for a big violation of the Lorentz-Berthelot (LB) combining rules (that was required in previous work⁴²). This violation destroys the predictivity of the model because extensive experimental data for the mixture would be required to determine a parameter describing the violation of the LB combining rule. Due to the generality of the approach and the level of accuracy for the pure components,¹⁰⁸ the present investigation is relevant both for practical purposes and for a general understanding of coarse graining procedures.^{43,44,45} We will also present results of an analytical Equation of State (EOS) which (apart from some region of the phase diagram near critical points) is able to yield rather satisfactory predictions in agreement with Monte Carlo results. It is very important to note that this EOS uses the same model parameters as the Monte Carlo simulation. This implies that in principle we are in a position to attempt to predict the phase diagram of a binary mixture (which is very complex^{38,39,40,41}) with comparatively small computational effort. In this view the reader should also interpret our choice to use LB combining rules: of course there are no reasons to believe that such approximations should be exact, and certainly there will be cases where more complicated

combining rules are preferable. However, the simple LB combining rules used here suffice for a wide class of systems with quite acceptable errors.

Due to the generality of the scheme presented in this work we expect discrepancies, and some regions of the phase diagram might not be predicted properly. This is related to several limitations of the present procedure like *i*) the large T expansion involved in the building of the CG model for quadrupolar solvents^{36,37} and *ii*) limitations related to our simple modeling approach like the simple potentials involved (Lennard-Jones), the neglect of atomistic details, and the use of the LB combining rules for which discrepancies are¹⁰⁹ known to arise (see e.g. 46 for some systems also investigated in this work). In order to disentangle point *i*) from point *ii*) we also present investigations of similar apolar mixtures for which the new CG model^{36,47} does not result in any improvement. The results show similar discrepancies from experiment as the polar phase diagrams, confirming the quality of the choice in Refs. 36,47. We want to stress that in order to test the goodness of our CG model, the only reliable method is a Monte Carlo investigation. Indeed, without MC simulation it is impossible to distinguish the bias related to the approximations involved in the EOS from the bias involved in the CG model [point *ii*) above]. For instance, we will present results for the mixture of methane and carbon dioxide for which EOS results will be in better agreement with experiments than MC results: this is clearly a fortuitous cancellation!

It is important to report that other interesting and significant attempts to build a systematic description of mixture phase diagrams are present in the literature. For instance in 48,49 mixtures are treated with models previously investigated in 50. For some of the molecules studied, these models allow for an additional parameter that can be adjusted and consequently a more accurate fit of experimental data is possible. On the other hand, there is a loss in predictivity because the full phase diagrams of the pure substances are required in order to determine the simulation parameters (computed in a χ square fit which minimizes discrepancies with experiment⁵⁰) plus mixture data^{48,49} to determine the mixing parameters.¹¹⁰ So the strategy of the present work is to deal with relatively simple models, where (in the framework of Monte Carlo simulations) the statistical mechanics can be dealt with at a very good level of accuracy (e.g. long runs employing advanced Monte Carlo techniques are possible to minimise statistical errors and systematic errors due to finite size effects which are avoided by finite size scaling analysis). These models are suitable for ana-

lytic EOS models as well, and can serve as a starting point for the coarse grained modeling of polymer solutions. Of course, we do not imply that a complementary simulation strategy (making models as detailed as possible, to account for the packing of molecules in the liquid as accurately as possible, including polarizability, etc.) is not worth pursuing in its own right, but it is outside of the scope of the present work.

II. COMPUTATIONAL DETAILS AND OUTLINE

It is well established^{5,19,20,21,22,42,52,53,54,55,56} that the most reliable approach to study the phase behavior of fluids is based on grand canonical Monte Carlo simulations together with histogram reweighting and finite size scaling techniques, especially if one wishes to include the critical region. In this study, we follow this approach, and amend it by successive umbrella sampling²⁴ to obtain coexistence curves far from criticality. This method has the additional advantage that the interfacial free energy between the coexisting phases can be extracted as well.^{57,58,59,60} As we are interested in a very fast simulation code, we omit any potentials including effective charges, and restrict our attention to short range effective potentials. Three-body (nonbonded) forces are avoided as well. Electrostatic quadrupole-quadrupole interactions are treated as a perturbation (which is practically justifiable³⁷), such that an effective angular-independent (but temperature-dependent^{36,37,61,62}) interaction decaying proportionally to the power r^{-10} of the interparticle distance r results. The dispersion forces are modeled by Lennard-Jones (LJ) potentials. For the sake of computational efficiency, all potentials are cut at the distance $r = r_c = 2(2^{1/6})\sigma$ and shifted to zero at r_c (σ is the range parameter of the LJ potential). When we deal with alkane chains, we disregard any torsional forces and bond-angle potentials and integrate a few successive chemical monomers into one effective monomeric unit (cf. fig. 1). This is done in the way that one such unit contains three carbon-carbon bonds between successive carbon atoms, and we do not distinguish between interior CH_2 monomers and the CH_3 groups at the chain ends. Thus, for example, hexadecane ($\text{C}_{16}\text{H}_{34}$) is represented by a chain molecule containing five effective monomers (see fig. 1).^{42,61} The procedure of coarsening three carbon atoms in a bead has been proven to be optimal in several theoretical investigations⁶³ (see Sec. 4.3.2). We stress that the particular choice of coarsening three carbon units into one bead has nothing to do with the physical lengths of the chain (like for instance the Kuhn length), but

is a choice that depends more on the potentials used. Indeed as neighboring beads along a chain interact with a bonding potential (see Sec. IIIC for definitions) in addition to the Lennard Jones potential, the coarse grained model of the chain exhibits a degree of local stiffness, although neither bond angle or torsional potentials are included explicitly. This implies that the Kuhn length is longer than the diameter of our beads.

Of course, the suitable choice of parameters is crucial for such coarse-grained models: we choose the strength of the quadrupole moment Q (if there is one) such that it is compatible with experimental data, and adjust the range σ and strength ϵ of the LJ potential such that the experimental critical density ρ_c and critical temperature T_c are reproduced precisely in the simulation. In Sec. III, we will briefly discuss the accuracy of this procedure for a variety of pure systems (noble gases, CO_2 , CH_4 , C_6H_6 , short alkanes) while Sec. IV contains the central part of our work, in which we present a variety of results for binary mixtures. The additional interactions needed for the mixtures are chosen by the simple Lorentz-Berthelot combining rules.⁶²

Technical aspects of our simulations are similar to previous studies.^{36,37,42} Far from the critical point coexistence densities are computed using the successive sampling algorithm of Virnau and Müller²⁴ in which high free energy barriers are overcome constraining the algorithm –at a certain time of the simulation– to sample configurations of a system where the number of particles is n or $n + 1$. Varying n from $n = 0$ to $n = N_{\text{MAX}}$ one is able to reconstruct (after proper reweighting) the free energy profile $F(n)$ at coexistence in the range of densities of interest. At phase coexistence, we expect a distribution $F(n)$ with two peaks (corresponding to the two coexisting phases that differ in particle number) which have equal weight. In few very fast runs (using a small cubic box $L \approx 7\sigma_M$, where σ_M is the biggest LJ length parameter of the model), invoking the equal weight rule for $F(n)$, we are able to tune the chemical potential(s) to their coexistence values, with a reasonable error ($\approx 1-5\%$) which in some cases should be enough. Then, we start a second long simulation for a larger elongated box (to enhance the formation of the liquid-gas interface) $V = 2 \cdot L^3$ with $L = 9\sigma_M$ in which every window is sampled with $2 \cdot 10 \cdot 10^4$ MC steps. Every MC step includes: 100 grand canonical moves in which we try to insert/delete solvent (and chain) particles, 1 local move in which a number of monomers equal to the total number of monomers are rearranged, and $10 \cdot N_{\text{chain}}$ reptation moves, where N_{chain} is the number of the chains in the box. Such a run requires on average 10 h of cpu time on 32 nodes of an IBM

Power4 cluster. The precision of the measured coexistence densities (for instance) is roughly 1%. Using a spherical averaged potential allows us to speed up computations by a factor $\approx 5^{37}$ in comparison with the full quadrupolar model. A number of chains $N_{\text{MAX}} \approx 1100$ usually allows a complete sampling of the liquid peak, while the number of solvent particles is typically of the same order of magnitude. We emphasize that –unlike simulations in the Gibbs-ensemble– in addition to the densities and compositions of the coexisting phases and their compressibilities, the simulation technique also provides information about the interface tension. At the critical point, we use the same kind of simulation described above, but unconstrained. (At every time the number of particles is free to fluctuate in all the region $[0, N_{\text{MAX}}]$). For more detail on the finite size analysis used we refer the reader to Sec. IVC.

Even with all these simplifying approximations, establishing the phase behavior and thermodynamic properties of binary mixtures comprehensively still requires a lot of work with Monte Carlo simulations. Far away from critical points, such an effort is not needed, and one can try to use an analytical equation of state. We use a previously developed theory based on Wertheim thermodynamic perturbation theory⁶⁴ (TPT). We strictly follow Ref. 65,66. In particular the free energy of the system A is decomposed in a contribution due to a mixture of unbonded monomers (the reference system) plus a contribution due to chain associativity A_{chain} ,⁶⁶ $A = A_{\text{ref}} + A_{\text{chain}}$. Wertheim’s theory allows us to compute A_{chain} perturbatively using quantities of the reference system (like pair correlation functions) and the known bonding potential. We use a first order perturbation theory (TPT1) which (at this point) reduces the problem to the computation of pair correlation functions and the free energy (A_{ref}) of a binary mixture of non-bonded monomers interacting with LJ potentials (chain-chain monomers and solvent-chain monomers) and the LJ + quadrupolar interaction (see Sec. IIIB) for solvent-solvent monomers. A_{ref} is computed using standard perturbation theory: the Ornstein-Zernike equation is solved using a Mean Spherical (MSA) closure.⁶⁷ In particular, one chooses as reference system a mixture of hard spheres with diameters computed using the repulsive part of the monomer-monomer potential in a Barker Henderson approximation,⁶⁸ while the attractive part of the potential is treated as a perturbation. A MSA solution is then obtained using the analytical implementation of Tang and Lu,^{69,70} in which the repulsive part of the LJ potential is fitted by a couple of Yukawa tails which allow to obtain an analytical result.⁶⁶ In our present modeling approach we need to consider

LJ potentials plus quadrupolar interactions. This problem has been solved in 36 (see App. A of 36) by applying a second pair of Yukawa tails to fit the quadrupolar interaction. In our MSA scheme we also use a “one fluid approximation”.⁶⁷ Our results will show how this simple theory is able to reproduce results in rather good agreement with MC data away from the critical point. On the other hand, big discrepancies occur near the critical points, due to the Mean Field nature of the MSA while experimental results exhibit critical behavior characteristic of the Ising universality class. We are aware of significant efforts to design proper EOS which include Ising fluctuation near the critical point.^{71,72} However, such investigations are beyond the scope of the present paper. Another popular method based on TPT1 is known as “statistical associating fluid theory” (SAFT).⁷³

We want to stress that Monte Carlo simulations remain an indispensable tool in investigations of the phase behavior of polymer solutions and mixtures. Indeed, in the present study the model parameters (ϵ , σ and q_c) have been determined³⁶ using the simulation critical points which were obtained by Monte Carlo simulation in 36. (Any mean field approximation has difficulties in reproducing the critical line with sufficient accuracy). Note that supercritical fluids are interesting and useful for practical applications, mainly due to their high compressibility and the concomitant large variations of density upon small changes of pressure, which are the origin of the breakdown of a mean field approximation like TPT. This means that in some very interesting regions of the phase diagram Monte Carlo simulations are indeed a very valuable tool.

III. PHASE BEHAVIOR OF SELECTED PURE SYSTEMS

When we discuss the extent to which the Lorentz-Berthelot combining rule can account for the phase behavior of mixtures, we need to distinguish between inaccuracies arising from an imperfect description of the pure components and those arising from the Lorentz-Berthelot rule. Therefore it is necessary to give an overview of our modeling of the pure components at the outset. Note that a possible additional source of errors are entropic packing effects of non-spherical molecules that may show up differently in a mixture of two molecules having different shapes rather than for a pure system, where all molecules have the same shape. Such effects are lost in our coarse-grained models. However, this latter criticism cannot be applied when we consider mixtures of noble gases, since in the framework of classical

statistical mechanics the description of noble gas atoms as point particles, where two such atoms interact with a potential depending on the absolute value of their distance only, is certainly appropriate. (Disregarding the case of He, quantum effects are negligible indeed at temperatures of interest⁷⁴). For that reason, noble gases are also included in our discussion, because they will bring out the possible limitations of our modeling in terms of pair-wise effective potentials between point-like particles most clearly. Thereafter, we shall deal with CO₂, C₆H₆, CH₄, and selected short alkanes.

A. Noble Gases

The interaction between neutral point-like particles in our work is always described by the Lennard-Jones (LJ) potential,

$$U_{ij}^{LJ} = 4\epsilon\left[\left(\frac{\sigma}{r_{ij}}\right)^{12} - \left(\frac{\sigma}{r_{ij}}\right)^6\right] \quad . \quad (1)$$

Rather than working with the full LJ potential as written in Eq. (1), we find it computationally more convenient and efficient to cut off this potential at $r = r_c = 2^{7/6}\sigma$ and shift it to zero there, such that

$$U_{ij}(r) = U_{ij}^{LJ}(r) + 4\epsilon S \quad , \quad U_{ij}(r \geq r_c) = 0 \quad , \quad (2)$$

where $S = 127/16384$ for our choice of r_c , so that the potential is continuous everywhere. When we require that Eqs. (1, 2) yield a vapor-liquid phase diagram such that the critical temperature T_c coincides with the experimental critical temperature T_c^{exp} of a particular system, the strength (ϵ) of the LJ potential is fixed once $T_c^* = k_B T_c / \epsilon$ has been determined for the model. Likewise, requiring that the critical density ρ_c of the model coincides with the experimental critical density ρ_c^{exp} of that system the range (σ) of the LJ potential is fixed once $\rho_c^* = \rho_c \sigma^3$ is known for the model. Here, $T^* = k_B T / \epsilon$ and $\rho^* = \rho \sigma^3$ are dimensionless temperature and density, respectively. Actually, the phase diagrams of both the full (untruncated) LJ potential and of its truncated version Eqs. (1, 2) have been estimated with high precision.^{42,59} Fig. 11 of Ref. 36 compares these phase diagrams with each other and with experimental data for the noble gases Ne, Ar, Kr and Xe.⁷⁵ One can see that in this scaled representation the differences between the phase diagrams based on full and truncated LJ models are quite minor. Although noble gases are thought to be the best

possible experimental realization of LJ fluids, the agreement is not perfect either: while Ne and Ar are very close to the LJ prediction, the data for the fluid branch of Kr and Xe are somewhat off. This implies that even noble gases do not strictly satisfy the “law of corresponding states”, and hence a description in terms of classical point particles interacting with purely pairwise potentials of the same functional form, $U_{ij}(r) = \epsilon f(r/\sigma)$, with one parameter for the strength (ϵ) and another for the range (σ) of the potential cannot be strictly true, irrespective of the form of the function $f(r/\sigma)$: either a more complicated form of the pairwise interaction, involving a third system-specific parameter is needed, or (what is usually assumed) some effect of three-body interactions^{76,77,78} are present.

An even more pronounced deviation from the simple LJ model shows up, however, when additional quantities are analyzed, such as the vapor pressure $p_{\text{coex}}(T)$ at liquid-vapor coexistence and the interfacial tension $\gamma(T)$ between the coexisting vapor and liquid phases of the fluid (see figs. 2, 3). It is clear that adjusting σ from ρ_c^{exp} implies that the whole curve for the coexistence pressure $p_{\text{coex}}(T)$ in the (p, T) plane is underestimated for both Kr and Xe. This is a serious drawback for the description of binary mixtures, of course, where one wishes to work in the (T, p, x) ensemble, x being the molar fraction of the solute. Therefore, we have tried an alternative, namely adjusting σ such that the experimental critical pressure $p_c^{\text{exp}} = p_{\text{coex}}(T_c)$ is correctly reproduced. For Kr the critical temperature $T_c^{\text{exp}} = 209.46 \text{ K}$ ⁷⁵ implies $\epsilon = 2.8971 \cdot 10^{-21} \text{ J}$. If one uses $\rho_c = 11.0 \text{ mol}/\ell$ ⁷⁵ to fit σ one obtains $\sigma = 3.6524 \text{ \AA}$, while using $p_c^{\text{exp}} = 55.20 \text{ bar}$ ⁷⁵ instead would yield $\sigma = 3.58782 \text{ \AA}$. (For a discussion of the accuracy of our estimation of ϵ and σ , we refer to table I. In order to guarantee the reproducibility of our results we always present ϵ and σ with all the digits that have been used in our programs.) Fig. 3 shows that a somewhat better description of the vapor pressure $p_{\text{coex}}(T)$ is obtained over the full temperature regime from $140\text{K} < T < T_c^{\text{exp}}$. The deviation from the data for the surface tension σ has also become smaller (fig. 2b), but now there is a strong deviation between the data for the liquid branch of the coexistence curve and the model (fig. 2a). Similar problems are observed for Xe, where $T_c^{\text{exp}} = 289.74\text{K}$ yields $\epsilon = 4.00747 \cdot 10^{-21} \text{ J}$, while the use of $\rho_c^{\text{exp}} = 8.371 \text{ mol}/\ell$ yields $\sigma = 4.00053\text{\AA}$ and use of $p_c^{\text{exp}} = 58.41 \text{ bar}$ yields $\sigma = 3.92326\text{\AA}$. Figs. 2, 3 show that for these noble gases the description of the coexistence curve, vapor pressure at coexistence and surface tension is clearly not as good as for the model of CO_2 and C_6H_6 proposed in Ref. 36. These problems carry over to our modelling of binary rare gas mixtures (see Sec. III A), as the comparison with

experimental data shows.⁷⁹ At this point we recall that as outlined in the introduction, the investigation of such a system has been undertaken in order to get an order of magnitude estimate of the errors inherent to our very simple models: the goal is not the derivation of a very elaborate description of noble gas mixtures. Figure 3 clearly shows that this model allows for a fairly good description of the mixture phase diagram (if compared to other mixtures presented in this work). In the present context it was not necessary to include more complex potentials available in the literature since long times (e.g. 80,81,82).

B. Small Molecules: Methane, Carbon Dioxide, Benzene

Methane (CH₄) is also described as a point particle, and again we take Eqs. (1), (2) as a coarse-grained description of the interaction between methane molecules. Using $T_c^{\text{exp}} = 130.6 \text{ K}^{75}$ and $\rho_c^{\text{exp}} = 10.1 \text{ mol}/\ell^{75}$ as experimental input to determine ϵ and σ , we obtain $\epsilon = 2.63624 \cdot 10^{-21} \text{ J}$ and $\sigma = 3.75792 \text{ \AA}$. Fig. 4 compares the resulting model prediction for the coexistence curve in the temperature-density plane, the vapor pressure at coexistence and the surface tensions with the corresponding experimental data.⁷⁵ It is remarkable that in this case the simple potential model {Eqs. (1), (2)} works better than in the case of the noble gas.

For molecules such as carbon dioxide (CO₂) and benzene (C₆H₆) the situation is more complicated: while CH₄ is a molecule of approximately spherical shape and does not have a quadrupole moment, both CO₂ and C₆H₆ have quadrupole moments. Note that (at least to a very good approximation^{83,84}) CO₂ is a linear molecule while C₆H₆ is disk-like. In 36 we have shown that a very good description for both molecules is obtained when Eqs. (1) are augmented, (2) by a quadrupole-quadrupole interaction term. As the latter is only a relatively small perturbation of the Lennard-Jones-type interaction, it suffices to treat the (angular-dependent) quadrupolar interactions via thermodynamic perturbation theory. To leading order this yields the following effective potential^{36,47,85}

$$U_{ij}^{IQQ} = -\frac{7}{5} \frac{1}{k_B T} Q^4 / r_{ij}^{10}. \quad (3)$$

Here, Q is the strength of the quadrupole moment of the considered molecule. Note that the interaction is isotropic and inversely proportional to temperature. We also cut off this part of the interaction at the same radius r_c as the LJ interaction, and shift it to zero at r_c

as well, which yields the following total pairwise interaction for these molecules

$$U(r_{ij}) = \begin{cases} 4\epsilon[(\sigma/r_{ij})^{12} - (\sigma/r_{ij})^6 - \frac{7}{20}q(\sigma/r_{ij})^{10} + S] , & r \leq r_c \\ 0 , & r \geq r_c \end{cases} \quad (4)$$

where

$$S = \frac{127}{16384} + \frac{7}{5} \frac{q}{256} \quad (5)$$

and q is the reduced quadrupolar interaction parameter,

$$q = Q^4/[\epsilon\sigma^{10}k_B T] = q_c T_c/T \quad , \quad q_c \equiv q(T_c) \quad . \quad (6)$$

Note that Eq. (6) is given in CGS units; in SI units, there would be an additional factor $(4\pi\epsilon_0)^{-2}$.

Using Eqs. (4)-(6), one can fix ϵ and σ such that critical temperature T_c^{exp} and density ρ_c^{exp} are reproduced. (For Q , the experimental value is taken as a first guess). As discussed in Ref. 36, this leads to a self-consistency problem, since Eq. (6) must hold together with

$$\epsilon(q_c) = k_B T_c^{\text{exp}}/T_c^*(q_c), \quad \sigma^3(q_c) = \left[\frac{\rho_c^*(q_c) M_{\text{Mol}}}{\rho_c^{\text{exp}} N_A} \right], \quad (7)$$

where M_{Mol} is the molar mass of the molecule and N_A is Avogadro's number. This problem was solved in 36 by determining the functions $T_c^*(q_c)/T_c^*(0)$, and $\rho_c^*(q_c)/\rho_c(0)$ by extensive Monte Carlo simulations for a broad range of values for q_c . It turns out that for CO_2 the experimental value $Q = 4.3 \pm 0.2 D \text{\AA}$ yields

$$q_c = 0.387, \quad \epsilon = 3.491 \times 10^{-21} \text{ J}, \quad \sigma = 3.785 \text{ \AA}, \quad (8)$$

while for the case of benzene the value $Q = 12 D \text{\AA}$ would imply

$$q_c = 0.247, \quad \epsilon = 6.910 \times 10^{-21} \text{ J}, \quad \sigma = 5.241 \text{ \AA} \quad . \quad (9)$$

The corresponding results for the vapor-liquid coexistence curves in the (T, ρ) and (p, T) planes as well as the temperature dependence of the interfacial tension for both CO_2 and C_6H_6 were already presented in 36 and shown to give a rather good agreement with experiments.⁷⁵

Of course, the disregard of the angular dependence of the quadrupolar part of the interactions is a matter of concern. This point was investigated by us in 37, where detailed comparisons of Monte Carlo results for the full angular-dependent quadrupole-quadrupole interaction and the isotropic approximation {Eqs. (3)-(6)} were performed for the case of CO₂. It was shown³⁷ that the model with LJ + full quadrupolar interactions (which is still a crude coarse-grained model, in comparison with all-atom models including partial charges etc.) does not provide a better account of the experimental data than the spherically averaged one.

Another point of concern is the possible sensitivity of the results of such models to the precise value of q_c . Note that q is proportional to Q^4 {Eq. (6)}. Consequently, a small experimental error in Q is magnified considerably. There may also be systematic effects since Q is often determined in the dilute gas phase. Here, we are interested in using densities around the critical density, and Q could be slightly renormalized there. Packing effects should also be taken into account. Indeed, CO₂ is not a spherical molecule, and at high density a local orientational order could arise. This packing could enhance some favorable angular correlations that give rise to a higher effective quadrupolar moment. One can argue that high temperature perturbative theory {see Eq. (3)} may not be very accurate and higher order terms could be important: in fact our previous investigation in which a full (angular dependent) quadrupolar interaction was considered,³⁷ proves that this is not the case. In addition, one may argue that the model of Eqs. (3)-(6) is an effective model, intended for a good representation of equation of state data, particular for vapor-liquid equilibria (VLE). Therefore, q_c should be treated as an effective parameter which can be used to optimize the description of such VLE data. In this spirit, we have also tried different choices of q_c and found that a slightly better description of CO₂ is obtained

$$q_c = 0.47 , \quad \epsilon = 3.349 \cdot 10^{-21} \text{ J}, \quad \sigma = 3.803 \text{ \AA}. \quad (10)$$

This choice was already included in our previous work.^{36,37} For benzene, a very good agreement with experiments can be achieved for

$$q_c = 0.38 , \quad \epsilon = 6.472 \cdot 10^{-21} \text{ J}, \quad \sigma = 5.284 \text{ \AA}. \quad (11)$$

Fig. 5 presents the coexistence curve of benzene in the $\rho - T$ and $T - p$ planes as well

as the interfacial tension. Results based on Eq. (11) are compared with results based on the previous choice {Eq. (9)}³⁶ and with experimental data.⁷⁵ The description of the experimental data is clearly remarkable over a wide range of temperatures. It turns out (see below) that these “optimized” choices of parameters {Eqs. (10), (11)} also yield a much better description when we consider mixing behavior (e.g. C₆H₆ + CH₄).

C. Short Alkanes

In this section we briefly discuss the extension of our methodology to systems such as propane (C₃H₈), pentane (C₅H₁₂) and hexadecane (C₁₆H₃₄). These short alkanes are just treated as test systems for our methodology and will be used in Sec. III as components in binary mixtures. Our methodology can be used, in principle, for any alkanes, provided information on the vapor-liquid critical point ($T_c^{\text{exp}}, \rho_c^{\text{exp}}$) is available. (Unfortunately, this is not the case for much longer chains).

As it was already emphasized (fig. 1) we do not attempt an all-atom description of alkanes. We also do not use an united atom model where CH₂ (or CH₃) groups are described as one spherical pseudo-atom.^{86,87} Such a model requires torsional and bond angle potentials and is still rather demanding to simulate. As indicated in fig. 1, we reduce the description to a coarse-grained bead-spring model, where a small number of successive CH₂ or CH₃ groups are combined into a single effective monomeric unit. For C₁₆H₃₄ we choose 5 effective units, so each unit contains about 3 C-C bonds. For pentane and hexane we choose a dimer (but the effective LJ parameters ϵ and σ are different, of course). Such a model is perhaps most questionable in the case of C₃H₈, which we treat as a single effective unit (i.e., such molecules are treated like almost spherically symmetric molecules such as methane).

We keep the (truncated and shifted) LJ potential {Eqs. (1), (2)} between all pairs of effective units, bonded and non-bonded ones. In addition we use the well-known FENE potential for the bonded ones⁸⁸

$$U_{\text{FENE}}(r) = -33.75\epsilon \ln[1 - (r/1.5\sigma)^2] \tag{12}$$

We note that in Eq. (12) ϵ and σ are the same parameters as in the LJ potential between the monomers. The parameters of the FENE potential have been chosen to prevent the crossing of macromolecules in the course of their motion. We note that this choice does not

reproduce the characteristic ratio of alkanes accurately. This means that the FENE potential is fully constrained, and the model remains a two parameter model with parameters chosen to match the critical temperature and density.

On this coarse-grained level both torsional potentials and bond-angle potentials between effective beads are ignored. Hence, it is worthwhile to test whether such crude models are still able to reproduce the phase diagram and other thermodynamic properties of the real system correctly. Thus, figs. 6-8 show results for the phase diagrams of several members of the alkane series (including C_3H_8 , C_5H_{12} and $C_{16}H_{34}$) in the T - ρ plane, as well as the corresponding coexistence pressures and interfacial tensions between the coexisting vapor and liquid phases. The agreement between the model results and the corresponding experimental data⁷⁵ is remarkable, again, although it is not as convincing as for methane (which we have included for comparison). In particular, for C_5H_{12} deviations clearly occur. Table I collects the experimental critical temperatures, densities, and pressures,⁷⁵ as well as our choices for ϵ and σ for the materials studied, and the prediction for the critical pressure that results from our model.

In all cases the critical pressure is predicted with an accuracy of a few percent, and a glance on Fig. 7 shows that the slope of the vapor pressure versus temperature curve is close to the slope derived from experiments, too. For temperatures away from the critical region (say, 20% below T_c), deviations between experiment and the model predictions become visible, both in the coexistence curve, coexistence pressure, and interface tension (Fig. 8), in particular for propane and pentane. Of course, the accuracy of the modeling could be enhanced by allowing for additional adjustable parameters like in many models in the literature, e.g. by introducing a bond-angle potential, or more interaction sites (see e.g. 45). Then, quantities such as the acentric factor (referring to the shape of the coexistence curve 30% below T_c ⁸⁹) can presumably be fitted nicely. However, the simplicity of the coarse-grained model is lost. Experience with such somewhat more complicated models shows that these models still require correction parameters ξ to the LB combining rules that deviate from unity by about 10% (see e.g. 49). Without these additional parameters (note that it is not at all straightforward to find optimal values for these parameters) the gain in accuracy that such models yield for the description of mixtures is rather modest. Note that an important motivation for the present work is to develop simple models suitable for the simulation of polymer solutions (the case of hexadecane in CO_2 being just a prototype case).

We are not focusing on pushing the accuracy of modeling of pure short alkanes to its limit.

IV. PHASE BEHAVIOR OF SELECTED BINARY MIXTURES

Extending our treatment to binary systems (A,B) one wishes to describe the interactions between unlike particles by a potential of the same functional form as it is used for the interactions between particles of the same type, i.e. the Lennard-Jones potential in our case. The simplest choice, most often used in the literature, is the Lorentz-Berthelot combining rule⁶²

$$\sigma_{AB} = (\sigma_{AA} + \sigma_{BB})/2, \quad \epsilon_{AB} = \sqrt{\epsilon_{AA}\epsilon_{BB}} \quad (13)$$

As is well-known, there is really no convincing derivation of Eq. (13), so there is no reason to believe that Eq. (13) is exact. At best it is a practically useful approximation. As a matter of fact, several alternatives to Eq. (13) have been proposed in the literature.^{62,90,91,92,93} Although it has been demonstrated that there are some cases where some of these alternative combining rules work better, in general none of these alternative combining rules has a really clear advantage.⁵² Since we wish to explore a very simple and general approach, we do not implement any alternatives to the simple Lorentz-Berthelot rule in our paper, even when one has to pay the price of sacrificing a small improvement in the accuracy of our modeling. We also note that the Lorentz-Berthelot rule works very well for the prediction of virial coefficients for the mixture of Argon plus CO₂, a mixture of an apolar and a quadrupolar fluid.⁹⁴ We want to stress that proceeding in such a way no experimental input from the mixture phase diagram is required for testing a full predictive model for the mixture. This also holds for the TPT1 computations which require only ϵ and σ that can be obtained using Monte Carlo results of the pure component critical line.³⁶ Coexistence densities and pressure have been computed as in pure component systems.²⁴ On the other hand, the computation of the critical points is more complicated. Indeed, in a binary mixtures close to criticality the proper identification of the order parameter is a subtle problem.⁹⁵ In principle, complete scaling^{96,97,98} in the case of binary mixtures implies that three scaling fields occur, which are linear combinations of four independent intensive variables: the deviations of two chemical potentials, temperature, and pressure from their values at the critical point. Consequently, the order parameter density becomes a function of the appropriate conjugate variable, and

the relevant physical densities (particle number densities, entropy density) become nonlinear functions of the proper scaling fields.⁹⁵ Since this formalism is somewhat cumbersome for the case of compressible binary fluid mixtures, we simplify the problem by applying “field-mixing”-procedures analogous to the method of Wilding^{19,20,21} which is rather successful for most one-component fluids. Details on this procedure are reported in the appendix A, presenting the analysis done for a critical point of the Krypton Xenon mixture. In order to estimate systematic errors of this procedure, in appendix A we also present results with a full finite size analysis with cumulants crossing¹⁶ for a highly asymmetric mixture like carbon dioxide in hexadecane.

A. Mixtures of Small Apolar Molecules

As a first example of apolar mixture we present results for krypton plus xenon. As it has been discussed in Sec. II, the noble gases already exhibit rather large deviations between the experimental data and the model calculations based on the Lennard-Jones potential. Thus, it is interesting to see whether these problems get even worse when mixtures are considered. The resulting critical line in the (p, T) plane is shown in fig. 3 for both choices of ϵ and σ as discussed in Sec. II A. If we fit ρ_c and T_c for the pure systems, the predicted critical points for the mixture deviate from the experimental curve about as much as for the pure systems. If we adjust ϵ, σ such that p_c, T_c is reproduced, the data⁷⁹ for the two mixed systems are almost perfectly reproduced. The variation of the critical concentration with temperature is also rather well reproduced (fig. 9) by both models where ρ_c and T_c or p_c and T_c are fitted to experimental values.

As a second case we consider now methane in butane. In Secs. II B, C we showed that the simple LJ model gives a fairly accurate account of the equation of state of both CH_4 and C_3H_8 . Therefore, it is natural to consider a mixture of those two molecules as a next step. Of course, a comprehensive study of the phase behavior of such mixtures in the space of all three variables (T, p, x) is a nontrivial effort. Therefore we limit ourselves to consider only isothermal slices through the phase diagram, following a standard practice in the literature.^{52,54} As an example, fig. 10 shows two such slices at $T = 327\text{K}$ (a) and $T = 277\text{K}$ (b), and compares experimental data⁹⁹ with selected Monte Carlo data and results from our implementation of the TPT1-MSA (which is described in appendix B of³⁶).

We emphasize that the various parameters characterizing the interactions among the various molecules are those obtained from Monte Carlo simulations of the pure materials (Sec. II), together with the Lorentz-Berthelot rule. These parameters also serve as input for TPT1-MSA: there are no additional parameters that enter the latter approach. Thus we present comparisons between experiments, simulations and theory in which no adjustable parameters for the mixture have been used.

It should be noted that both chosen temperatures in fig. 10 fall below the critical temperature of C_3H_8 but exceed the critical temperature of CH_4 . Therefore, the characteristic bubble-shaped liquid-vapor coexistence curve results, starting out at the ordinate axis at the vapor-liquid coexistence point of pure C_3H_8 , but not extending to CH_4 concentrations close to $x = 1$. The critical point occurs at the maximum of this closed loop. (The liquid phase is located on the upper part of the loop to the left of the critical point, the remaining part of the curve describes the vapor). For $T = 327\text{K}$ and $x \leq 0.35$ both experiment, TPT1 and Monte Carlo agree nicely. For larger x , however, a systematic discrepancy between Monte Carlo data and experiment shows up. The TPT1-MSA approximation overestimates the critical pressure substantially. This problem already occurs in the pure systems, as is well-known, and is an inevitable consequence of simple mean-field-like approximations.^{36,63,65} Fig. 4 shows that the critical temperature and pressure of pure CH_4 are both overestimated. The same holds for pure C_3H_8 , and the whole line of critical points $T_c(x)$ that connects $T_c(0)$ and $T_c(1)$ when we would project them into the (p, T) plane as we did for the Kr-Xe mixture (fig. 3). As in the latter case, the mixture of CH_4 and C_3H_8 has a simple “type I” phase diagram in the classification scheme of fluid binary mixtures^{38,39,40} (type 1^P in the modern classification⁴¹). As a consequence, we expect that TPT1-MSA predicts too large vapor-liquid coexistence loops in the (p, x) plane at all temperatures that are supercritical for CH_4 but subcritical for C_3H_8 .

A more disturbing discrepancy seems to occur between the data⁹⁹ and the theoretical results at the lower temperature ($T = 277\text{K}$), where at small x the vapor pressure at coexistence falls slightly but systematically below the experimental data. For molar concentrations well below criticality, Monte Carlo results and TPT1-MSA agree very well, and our numerical procedures are accurate for our model. Hence, assuming that the experimental data are accurate enough so that the discrepancy is meaningful, this result indicates that some limitations of our model become apparent. This is not really a surprise, of course, because

in the data for pure propane at this temperature discrepancies of the order of a few percent do occur as well (figs. 6-8).

As a third case we now consider the mixture of CH_4 , and C_5H_{12} , because for pentane slightly larger deviations between the predicted and observed coexistence vapor pressure do occur over a much broader temperature range (fig. 7). Indeed, the corresponding isothermal slices through the phase diagram of that mixture (fig. 11), which still is a type-I phase diagram, show that slight but systematic discrepancies are now seen at the higher temperature as well. At the low temperature, the phase diagram can only be reproduced in a rather qualitative manner. Note, however, that $T = 237\text{K}$ is less than 50% of the critical temperature of pentane, where the effective interactions of pentane were adjusted: of course, the coarse-grained modelling used in our work should not be pushed to too low temperatures. Keeping this limitation in mind, we conclude that a rather satisfactory description of mixing behavior of these systems is in fact reached by our models. Hoping for perfect agreement would have been premature, in view of the simplicity of our models. But the phase diagram predictions should allow a useful first orientation at temperatures not too far below of the higher critical temperature of the components in such a binary mixture.

B. Mixtures of small molecules, one of which has a quadrupole moment

We begin with a mixture of CH_4 and CO_2 , because for both pure molecules a particularly accurate description of the equation of state was obtained (see Sec. II). Again we note that the $\text{CH}_4 + \text{CO}_2$ system belongs to the category of “type I” phase diagram in the classification scheme of Scott and van Konynenburg^{38,39,40} (1^P in the modern classification⁴¹) and the temperature regime of interest for our modeling is the regime in between the critical temperatures of the two constituents of this mixture. Note that Eq. (13) only applies to the LJ part of the interactions of CO_2 , since CH_4 has no quadrupole moment.

In fig. 12 we present isothermal slices through the phase diagram in the space of variables (T, p, x) . If one uses TPT1-MSA the model for CO_2 based on Eq. (10) can describe the mixing behavior with CH_4 very accurately at molar concentrations x of CH_4 and pressures that are not close to criticality. As emphasized above, mean-field theories such as TPT1-MSA are not expected to be accurate near critical points. Hence, the discrepancy that TPT1-MSA predicts a too large loop inside of which two-phase coexistence occurs, is inevitable and

expected. But for the model Eq. (10) the part of the loop at not too large x is significantly more accurate (full curves) than a simple LJ model for CO_2 would be (broken curves). As expected, at low temperatures (such as $T = 230\text{K}$) the quadrupolar model for CO_2 {Eq. (8)} also starts to show slight but systematic deviations from the experiment at the vapor branch of the vapor-liquid coexistence curve. This is similar to our finding for the apolar mixtures (Sec. III B).

In order to verify that the good agreement between experiment and theory for the quadrupolar model of CO_2 in the $\text{CH}_4 + \text{CO}_2$ mixture is not just fortuitous, we show in fig. 13 corresponding results for the mixture of benzene (C_6H_6) and methane (CH_4). This is a more stringent test, since the critical temperatures of the two constituents are rather far apart from each other (cf. figs. 4, 5). Nevertheless, the conclusions are the same as in the case of $\text{CH}_4 + \text{CO}_2$: using interaction parameters that were optimized for the pure systems, namely those of Eq. (11) in the case of C_6H_6 , and adjusting them to Monte Carlo results as described in Sec. II, we can proceed to the description of the mixture data¹⁰³ and estimate the missing mixed interaction parameters from the Lorentz-Berthelot rule, Eq. (13). The use of these interaction parameters in a simple and fast analytical theory for the EOS such as TPT1-MSA then provides a satisfactory description of the phase behavior of the mixture, apart from the vicinity of critical points (this drawback can be rectified by carrying out MC work for the mixture as well, of course) and for not too low temperatures. (For temperatures of the order of 50% of the critical temperature T_c of the constituent with the higher T_c systematic deviations start to appear rather generally.)

The last example of this section deals with a slightly more complicated case, namely the $\text{CO}_2 + \text{C}_5\text{H}_{12}$ system (fig. 14): while CO_2 is still represented as a point particle with a quadrupole moment, as in the previous examples, the other partner of this mixture (C_5H_{12}) should not be coarse-grained into a point particle any more, but rather needs to be represented as a dimer (i.e., a dumbbell-like effective molecule). In this case the TPT1-MSA theory predicts unmixing over a far too large range of molar CO_2 concentrations, and the improvement provided by the inclusion of the quadrupolar moment at small x is only qualitative, but not quantitative. On the other hand, the Monte Carlo results for this model are in rather good agreement with the corresponding experimental data.¹⁰⁴ Since MC and TPT1-MSA are using precisely the same interaction parameters, we conclude that for this particular case TPT1-MSA is somewhat inaccurate for the vapor branch of the mixture,

far away from criticality. A related discrepancy was already noted for the $\text{CH}_4 + \text{C}_5\text{H}_{12}$ system at $T = 378\text{K}$ (fig. 11a). Perhaps this indicates that TPT1-MSA does not capture the statistical mechanics of flexible dimers well enough.

C. Polymer solutions: The $\text{CO}_2 + \text{C}_{16}\text{H}_{34}$ system revisited

Virnaeu et al.^{42,55,56} already attempted to model this system, describing CO_2 as a point particle with no quadrupole moment. They found that using the Lorentz-Berthelot rule {Eq. (13)} the phase diagram predicted by the model belongs to type I, while experiments suggest^{103,105} that this system belongs to the type III class (1^C1^Z , according to 41, where 1^C means that the critical line emanating from the pure component critical point of the hexadecane goes to high pressure regions without joining the solvent critical point like in diagrams starting with 1^P). Virnaeu et al.⁴² proposed that one can improve the description by using an empirical factor ξ to modify Eq. (13), assuming that $\epsilon_{AB} = \xi\sqrt{\epsilon_{AA}\epsilon_{BB}}$ instead of $\epsilon_{AB} = \sqrt{\epsilon_{AA}\epsilon_{BB}}$. In the literature, the value of ξ depends on the specific mixture and typically is written in the form $\xi_{AB} = 1 - k_{AB}$, with $k_{AB} \geq 0$. Of course, there is not really a theoretical justification for doing so, and ξ simply plays the role of a fitting parameter. By trial and error it was found that $\xi = 0.886$ provides a description compatible with the experimental data.

In the present subsection of our paper, we show that the main source of the problems encountered in 42 was the neglect of the quadrupole moment. Thus, we have repeated the study of the $\text{CO}_2 + \text{C}_{16}\text{H}_{34}$ system, insisting on the Lorentz-Berthelot rule, Eq. (13), but using Eq. (10) as an improved model for CO_2 , as in the previous subsection. Again, the Lorentz-Berthelot rule is only applied to the Lennard-Jones part of the interactions, since $\text{C}_{16}\text{H}_{34}$ does not have a quadrupole moment.

Following the strategy of the previous subsection, we have computed an isothermal slice through the phase diagram at $T = 486\text{K}$, where data from the previous simulation⁴² were available both for $\xi = 1$ and for $\xi = 0.886$. Indeed it is found that the data of the present model ($\xi = 1$, but optimized quadrupolar interaction $q_c = 0.47$ for pure CO_2) are well compatible with the experimental data¹⁰⁶ and almost fall on top of the results of the previous calculation with $q_c = 0$ and $\xi = 0.886$.⁴²

Of course, we have already seen in the previous subsections, that often a very good

agreement between our description based on a very simplified model occurs at high enough temperatures. In order to test, to what extent this problem arises for the present system, we have followed the strategy of 42 to compute the full critical line $T_c(x), p_c(x)$ for the full range of molar concentrations x of CO_2 . Fig. 16 shows the resulting projection into the p^*, T^* plane. (Here p, T are given in LJ units, with the LJ parameters of the effective monomers used to rescale the variables). One sees that the simulations with nonzero quadrupole moment included in the figure are close to those for $\xi = 0.9, q_c = 0$, for $T^* \leq 1.3$. As a consequence, the model that we have developed for CO_2 , Eq. (10), is still not able to yield the correct phase diagram topology. (For $\xi = 0.9$, transition type IV was observed in Ref. 42, as opposed to type III which was observed experimentally.) For $T^* < 0.8$ the model does not yet describe the properties of hexadecane + carbon dioxide mixtures accurately, although for $T^* \geq 1.3$ ($T \geq 545\text{K}$) the properties of the system are predicted rather satisfactorily. Of course, this result is not unexpected. For $T \leq 0.5T_c^{hex} \approx 360\text{K}$ the model based on fitting the critical parameters of hexadecane to fix its interaction parameters starts to become inaccurate. On the other hand, the proper prediction of the phase diagram type is a very stringent test. Indeed, variation of the interaction parameters by a few percent could drastically change the type of the phase diagram.⁴²

V. CONCLUSIONS

In this paper, we have studied the phase diagrams of a variety of fluid binary mixtures, with particular emphasis on mixtures of alkanes in supercritical carbon dioxide and benzene. In order to better understand the performance of our modeling for these systems, we have also investigated mixtures with apolar solvents including noble gases and methane. We have investigated the accuracy of the use of the Lorentz-Berthelot rules for describing the mixing behavior, based on interaction parameters for the pure systems that are tuned such that the critical point (critical temperature, critical density or pressure) of the pure systems are well reproduced. Using a simple Lennard-Jones model for interaction parameters of pure apolar fluids, Monte Carlo calculations in the grand-canonical ensemble, analyzed by appropriate finite size scaling methods, readily yield the desired accuracy for this procedure. For the polar molecules we use a spherically averaged point-like quadrupolar interaction,^{36,47,85} which was shown to produce very good phase diagrams,³⁶ also if compared to more realistic

atomistic models. Our model takes as experimental input the critical temperatures and densities of the pure components (like in previous coarse grained schemes⁴²) plus the experimental quadrupolar moments. For pure CO₂ and C₆H₆ this choice leads to a significant improvement in comparison with a simple LJ model without explicitly accounting for the polar interactions. In Ref. 36 and Fig. 5, as a second option, we have treated the quadrupole moment as an effective parameter in an attempt to optimize agreement with experiments. We tune this parameter such that the liquid branch of the vapor-liquid coexistence curve of pure CO₂ or pure C₆H₆ is optimally represented. In the case of benzene, for which the optimization procedure seems to work very well, the agreement with the coexistence pressure is also improved. (This is not the case of CO₂ which is however better described than benzene if the experimental values for the quadrupole moments are used.) The physical reason for this requirement to work with an effective quadrupole moment is presumably that actual molecules are not point-like particles, of course: CO₂ is a rather elongated molecule, while C₆H₆ is disk-like. So packing effects should occur, i.e. local orientational correlations, which are underestimated by the quadrupolar interaction. Thus, it is gratifying to note that a remarkable improvement of accuracy in the prediction of the phase behavior of mixtures is achieved if this effective quadrupole moment is used.

These energy parameters, which we fixed from the description of the pure systems, together with the Lorentz-Berthelot rules, allow us to predict phase diagrams of mixtures, with no ambiguity whatsoever, since no further adjustable parameters occur. Two methods of prediction are used: (i) Monte Carlo simulations (ii) TPT1-MSA calculations. The Monte Carlo approach has the substantial advantage that it is also accurate near critical points of the mixture. In principle, we obtain the exact statistical mechanics of the model system. Any discrepancy between experiment and prediction is entirely due to a shortcoming of the (simplified) model. The TPT1-MSA approach has the merit that relatively little computational effort is necessary to implement it. However, it clearly involves various approximations and hence the interpretation of discrepancies between TPT1-MSA and experiment is not so clear - part of them being due to inadequacies of the model, part of them stem from inaccurate approximations. For instance, TPT1-MSA, like all mean-field theories, overestimates the critical temperature and pressure, so the isothermal slices through the phase diagram of the mixture always involve two-phase regions which are too large.

We note that fluids like CO₂ have an important application as supercritical solvents. If

one aims at describing the behavior in the critical region of the pure solvent and of the mixtures correctly, Monte Carlo methods have a clear advantage. Now, one could try to readjust parameters in the TPT1-MSA approach to improve agreement with experiment (like done for instance in 66, where ϵ and σ for the EOS have been rescaled in comparison to the model used in MC simulations in order to properly reproduce the critical points of the pure compounds), but this would be just an attempt to provide a partial cancellation of errors, and in other regions of the phase diagram the description would necessarily get worse.⁶⁶ Since we feel that relatively little physical insight is gained by such fitting procedures, they have not been implemented in our paper. Our overall conclusion is that in the framework of the modeling as defined above the Lorentz-Berthelot rules work very well, in the sense that an ad-hoc change of mixed binary interactions by at most a few percent (typically one or two percent) would lead to almost perfect agreement with experiment. As a piece of evidence for this claim, we note that in the study of the $\text{CO}_2+\text{C}_{16}\text{H}_{34}$ system by Virnau et al.,⁴² where the CO_2 molecule was modeled as a point particle with LJ interactions with no account of the quadrupole moment, a correction factor $\xi = 0.886$ to the Lorentz-Berthelot rule was required to produce good agreement with experiment. However, the present model (with a quadrupolar interaction and no correction factor) yields results that are almost identical to those of Virnau et al.⁴² when $\xi = 0.900$ is chosen. As a consequence, we conclude that in the present model a correction factor $\xi \approx 0.985$ would suffice to reproduce the results. Noting that the Lorentz-Berthelot rule assumes that the mixed correlation functions in the fluid described atomistically behave in the same way as in the coarse-grained descriptions, deviations of such a fitting parameter ξ from unity in the range from 1 to 2% are no surprise at all.

Thus we feel that the present level of accuracy cannot easily be improved in the framework of our model. As it has been emphasized already in the introduction, many more complicated models for fluids are discussed in the literature (see 28,29,30,31,32,33,107). Optimizing parameters in those models such that the critical properties of the pure systems and their vapor-liquid coexistence curves are very well reproduced, might be an alternative starting point to test the validity of combining rules.^{48,49,50} However, even for our very simple model the Monte Carlo runs require substantial computer resources, and hence we have not attempted to generalize our approach to other models. The strength of our method, if compared to more detailed models with a lot of parameters the optimization of which would

require massive computation, is its generality. It is possible to have the potentials for a given mixture, without any extra computational efforts from the results of the pure components.³⁶ It is also important to mention that the present work validates the use of spherical averaged quadrupolar potential.^{36,47,85}

Finally, it is important to observe that our way to coarse grain solvent molecules into single beads has the advantage, with respect to atomistic models like multi center Lennard Jones, to be accessible to advanced equation of state machineries. In this paper we have shown how, with rather small efforts, significant results can be obtained. We are also aware of the fact that several improvements could be done (e.g. using some integral equation scheme which should improve the MSA solution near the critical point). However, most of the advanced methods in equation of state modeling, apply only for reference systems that are mixture of monomers (i.e. beads with point-like interactions), the associating part being taken into account by TPT1. On the other hand TPT1 gives a reasonable description only if in the “associated molecule” diameters of the beads do not overlap. This is of course the case in our CG model for alkanes in which the experimental distance between three carbon units ($d=4.59 \text{ \AA}$) is bigger than the typical σ used ($\sigma \approx 4 \text{ \AA}$). (This is another reason the FENE potential uses the same simulation parameters of the LJ interaction.) The condition $d > \sigma$ guarantees that the reference system (a mixture of monomers) is a good starting point for a perturbation theory. On the other hand if $d < \sigma$ association is too strong and cannot be properly taken into account by TPT1 (i.e. the monomer reference system is not the adequate starting point for a perturbation expansion). In models which describe simple solvent molecules with several interacting points (see e.g. Tab. 1 of 50 for typical parameters of two center LJ) we have $d < \sigma$: this implies that these models cannot be investigated with associating theories. In conclusion, our modeling approach might enable the application of modern EOS which is another important motivation of our work.

We do feel that the approach based on the present models is able to make nontrivial and practically useful predictions for a large class of systems. Hopefully more experimental data on mixtures will become available to allow for more stringent tests.

ACKNOWLEDGEMENTS CPU times was provided by the NIC Jülich and the ZDV Mainz. We would like to thank M. Oettel (University of Mainz), F. Heilmann and H. Weiss (BASF AG, Ludwigshafen) for fruitful discussions. BMM would also like to

acknowledge BASF AG (Ludwigshafen) for financial support. LGM wishes to acknowledge support from Ministerio de Educacion y Ciencia (project FIS2007-66079-C02-01) and Comunidad Autonoma de Madrid (project MOSSNOHO-S0505/ESP/0299).

APPENDIX A: DETERMINATION OF THE CRITICAL POINT

In this appendix we describe how the critical points for the mixtures (e.g. figs. 3-16) have been obtained. As mentioned in the sec. IV in asymmetric binary mixtures the determination of the order parameter is difficult⁹⁵ and a complete scaling^{96,97,98} requires a lot of work which has to be repeated for every critical point. For this reason in the present work the method of Wilding^{19,20,21} has been used. Taking as an example the krypton-xenon mixture (but the same procedure has been done for all the other mixtures), we take the order parameter M as a linear combination of the particle numbers of Kr atoms (N_k) and of Xe atoms (N_x) and of the total potential energy E_{tot}

$$M = N_x + x_1 N_k + x_2 E_{tot} , \quad (\text{A1})$$

where the parameters x_1, x_2 are determined by the following iterative procedure. First, the chemical potential μ_x^* (in LJ units) is tuned to get vapor-liquid phase coexistence (i.e., the distribution $P(M)$ satisfies the equal area rule). Normally, due to the lacking of the particle-hole symmetry, the two peaks will not be symmetric such as the two peaks of the universal Ising model distribution at criticality. Thus, as a second step the other chemical potential is also tuned (and the step 1 is repeated), so that one gets somewhat closer to the critical point of the system. Still, the universal shape of the distribution is not yet obtained. The third step consists in a variation of x_1 (and repeating steps 1 and 2) such that the two peaks of the distribution become as similar to each other as possible. The fourth step amounts to a variation of x_2 (again repeating steps 1 and 2). In this way (for the investigated cases) it is possible to obtain a final histogram of the order parameter M that reproduces the universal Ising shape at criticality almost exactly (fig. 17).

On the other hand the previous approach is not totally correct because it neglects finite size corrections for the critical parameters but simply “supposes” that the simulation box is large enough. In order to elucidate this point in this appendix we also report the full finite size analysis¹⁶ with crossing cumulants for several simulation boxes. We do this investigation

for the polymer solution studied in this paper ($\text{CO}_2 + \text{C}_{16}\text{H}_{34}$) which should be more sensible to mixing effects being a highly asymmetric mixture in which the coupling between two order parameters (total density and relative concentration, respectively) may be more of a problem rather than for some noble gas or small molecule mixtures. In fig. 18 we report our finite size analysis for the critical point at $T=486$ K. From extensive $\mu_s\mu_pVT$ simulations (μ_s being the chemical potential of the solvent, CO_2 in this case, and μ_p the chemical potential of the polymer $\text{C}_{16}\text{H}_{34}$) histograms have been generated for the total energy E_{tot} , the number of solvent particles N_s and the number of polymers, N_p . The probability distribution for the order parameter $M = N_p + x_1N_s + x_2E_{tot}$ is computed, using $x_1 = 0.08$ as an initial guess (it turns out that the final results depend on the parameter x_2 so weakly, that one may choose $x_2 = 0$ here; on the other hand the choice $x_1 = 0.08$ was suggested comparing $P(M)$ with the universal Ising curve, similarly to what has been done above for the Krypton-Xenon mixture). The simulation box linear dimensions were $L = 9\sigma_p$, $L = 11.3\sigma_p$ and $L = 13.5\sigma_p$. For a fixed x_1 and μ_s , μ_p is always fixed so that $P(M)$ satisfies the equal area rule. Then, we compute second and fourth order cumulants $B_2 = \langle \mathcal{O}^2 \rangle / \langle |\mathcal{O}| \rangle^2$, $B_4 = \langle \mathcal{O}^4 \rangle / \langle \mathcal{O}^2 \rangle^2$ (where $\mathcal{O} = M - \langle M \rangle$) as a function of μ_s , for different L (fig. 18a). It is seen that rather well-defined intersection points of the curves B_2 and B_4 vs. μ_s for different choices of L do in fact occur at $\mu_s = -2.058 \pm 0.001$. Using a simple comparison with the universal critical curve (which is the method we have used for all the critical lines of fig. 16) we previously obtained a value $\mu_s = -2.06$, which is very close to the value determined above (in particular within the 0.5% which is our general estimate of errorbars). The intersection for B_2 occurs close to the theoretical value²¹ $B_2^* = 1.22382$, while the intersection point for the curves B_4 is somewhat too low. This may indicate that the choice of the mixing parameter x_1 is not optimal. However, varying B_4 as a function of x_1 , at fixed choices of μ_s we observe that B_4 has a shallow minimum near the chosen value $x_1 = 0.08$ (see inset of fig. 18a). This could justify in some sense the a priori chosen value for x_1 and gives an estimate of the systematic error related to the choice of x_1 , which is very small. (We notice that variation of B_4 with x_1 is not strong enough that one could tune the parameters such that the intersection occurs strictly at the theoretical value, and with a distribution function $P(M)$ which is far from looking like the Ising curve). We conclude that all the sizes from $L = 9\sigma_p$ up to $L = 13.5\sigma_p$ are not yet in the asymptotic region of finite size scaling, and so various corrections to finite size scaling occur which could only be disentangled if a much wider range of L were at our

disposal. In view of such possible systematic errors, we have allowed an error bar for the critical values of μ_s and μ_p of 3 parts in a thousand, three times as large as one would conclude from a naive analysis of fig. 18a. In any case, the uncertainties resulting from these finite size analysis are much less than the deviation between our model predictions and the experimental data.

-
- ¹ D. Levesque, J.-J. Weis, and J. P. Hansen, in *Monte Carlo Methods in Statistical Physics*, edited by K. Binder (Springer, Berlin, 1979), p. 47.
- ² D. Levesque, J.-J. Weis, and J. P. Hansen, In *Applications of the Monte Carlo Method in Statistical Physics*, edited by K. Binder (Springer, Berlin, 1984), p. 37
- ³ D. Levesque and J.-J. Weis, in *The Monte Carlo Method in Condensed Matter Physics*, edited by K. Binder (Springer, Berlin, 1992), p. 121
- ⁴ D. Frenkel and B. Smit, *Understanding Molecular Simulation: From Algorithms to Applications* (Academic Press, San Diego, 1996)
- ⁵ N. B. Wilding, in *Computer Simulations in Condensed Matter: From Materials to Chemical Biology, Vol. 1* edited by M. Ferrario, G. Ciccotti, and K. Binder (Springer, Berlin, 2006), p. 39; M. Müller and J. J. de Pablo, **ibid** p. 67.
- ⁶ A. Z. Panagiotopoulos, *Molec. Physics* **61**, 813 (1987)
- ⁷ A. Z. Panagiotopoulos, N. Quirke, M. Stapleton, and D. J. Tildesley, *Molec. Phys.* **63**, 527 (1988)
- ⁸ A. Z. Panagiotopoulos, *Molec. Simulation* **9**, 1 (1992)
- ⁹ J. L. Siepmann and D. Frenkel, *Molec. Phys.* **75**, 59 (1992)
- ¹⁰ D. Frenkel, G. C. A. M. Mooji, and B. Smit, *J. Phys.: Condens. Matter* **4**, 3053 (1992)
- ¹¹ J. J. de Pablo, M. Laso, and U. W. Suter, *J. Chem. Phys.* **96**, 2395 (1992)
- ¹² A. M. Ferrenberg and R. H. Swendsen, *Phys. Rev. Lett.* **61**, 2635 (1988)
- ¹³ A. M. Ferrenberg and R. H. Swendsen, *Phys. Rev. Lett.* **63**, 1195 (1989)
- ¹⁴ R. H. Swendsen, J. S. Wang, and A. M. Ferrenberg, in *The Monte Carlo Method in Condensed Matter Physics*, edited by K. Binder (Springer, Berlin 1992), p. 75.
- ¹⁵ M. E. Fisher, in *Critical Phenomena*, edited by M. S. Green (Academic, London, 1971), p. 1
- ¹⁶ K. Binder, *Z. Physik B***43**, 119 (1981)

- ¹⁷ K. Binder, in *Computational Methods in Field Theory*, edited by C. B. Lang and H. Gausterer (Springer, Berlin, 1992)
- ¹⁸ K. Binder, Rep. Progr. Phys. **60**, 487 (1997)
- ¹⁹ N. B. Wilding and A. D. Bruce, J. Phys.: Condens. Matter **4**, 3087 (1992)
- ²⁰ N. B. Wilding, Phys. Rev. E**52**, 602 (1995)
- ²¹ N. B. Wilding, J. Phys.: Condens. Matter **9**, 585 (1997)
- ²² J. Perez-Pellitero, P. Ungerer, G. Orkoulas and A. D. Mackie, J. Chem. Phys. **125**, 054515 (2006)
- ²³ G. M. Torrie and J. P. Valleau, J. Comp. Phys. **23**, 187 (1977)
- ²⁴ P. Virnau and M. Müller, J. Chem. Phys. **120**, 10925 (2004)
- ²⁵ B. A. Berg and T. Neuhaus, Phys. Lett. B**267**, 249 (1991); Phys. Rev. Lett. **68**, 9 (1992)
- ²⁶ A. P. Lyubartsev, A. A. Martsinovska, S. V. Shorbunov and P. N. Vorontsov-Velyaminov, J. Chem. Phys. **96**, 1776 (1992)
- ²⁷ F. A. Escobedo and J. J. de Pablo, J. Chem. Phys. **105**, 4391 (1996)
- ²⁸ H. J. Böhm and R. Ahlrichs, Molec. Phys. **55**, 445 (1985)
- ²⁹ M. G. Martin and J. I. Siepmann, J. Phys. Chem. B**103**, 4508 (1999); *ibid* **102**, 2569 (1998)
- ³⁰ R. Bukowski, J. Sadlej, B. Jeziorski, P. Jankowski, K. Szalewicz, S. A. Kucharski, H. L. Williams, and B. M. Rice, J. Chem. Phys. **110**, 3785 (1999)
- ³¹ S. Bock, E. Bich, and E. Vogel, Chem. Phys. **257**, 147 (2000)
- ³² J. Yang, Y. Ren, A. Tian, and H. Sun, J. Phys. Chem. B**103**, 4508 (1999); *ibid***102**, 2569 (1998)
- ³³ Z. Zhang and Z. Duan, J. Chem. Phys. **122**, 214507 (2005)
- ³⁴ *Supercritical Fluids*, edited by E. Kiran and J. M. H. Levelt-Sengers (Kluwer, Dordrecht, 1994)
- ³⁵ *Supercritical Carbon Dioxide in Polymer Reaction Engineering* edited by M. F. Kemmere and Th. Meyer (Wiley-VCH, Weinheim, 2005)
- ³⁶ B. M. Mognetti, L. Yelash, P. Virnau, W. Paul, K. Binder, M. Müller, and L. G. MacDowell, J. Chem. Phys. **128**, 104501 (2008)
- ³⁷ B. M. Mognetti, M. Oettel, L. Yelash, P. Virnau, W. Paul, and K. Binder, Phys. Rev. E **77**, 041506 (2008)
- ³⁸ R. L. Scott and P. H. van Konynenburg, Discuss. Faraday Soc. **49**, 87 (1970)
- ³⁹ P. H. van Konynenburg and R. L. Scott, Philos. Trans. R. Soc. London Ser. A**298**, 495 (1980)

- 40 J. S. Rowlinson and F. L. Swinton, *Liquids and Liquid Mixtures* (Butterworths, London, 1982)
- 41 A. Bolz, u. K. Deiters, C. J. Peters, and T. W. de Loos, *Pur. Appl. Chem.* **70**, 2233 (1998)
- 42 P. Virnau, M. Müller, L. G. MacDowell, and K. Binder, *J. Chem. Phys.* **121**, 2169 (2004)
- 43 *Coarse-Graining of Condensed Phase and Biomolecular Systems*, edited by G. Voth (Taylor and Francis, in press)
- 44 *Handbook of Material Modeling*, edited by S. Yip (Springer, Berlin, 2005)
- 45 *Simulation Method for Polymers*, edited by M. J. Kotelyanskii and D. Y. Theodorou (Marcel Dekker, New York, 2004)
- 46 C. P. Hicks, R. L. Hurle, C. L. Young, *J. Chem. Soc.-Far. Tran. II* **73**, 1884 (1977).
- 47 E. A. Müller, and L. D. Gelb, *Ind. Eng. Chem. Res.* **42**, 4123 (2003)
- 48 J. Stoll, J. Vrabc, and H. Hasse, *AIChE* **49**, 2187 (2003).
- 49 J. Vrabc, J. Stoll, and H. Hasse, *Mol. Sim.* **31**, 215 (2005).
- 50 J. Vrabc, J. Stoll, and H. Hasse, *J. Phys. Chem. B* **105**, 12126 (2001).
- 51 J. G. Harris and K. H. Yung, *J. Phys. Chem.* **99**, 12021 (1995)
- 52 J. J. Potoff, J. R. Errington, and A. Z. Panagiotopoulos, *Molec. Phys.* **97**, 1073 (1999)
- 53 J. Delhommelle, A. Boutin, and A. H. Fuchs, *Molec. Simulation* **22**, 351 (1999)
- 54 J. J. Potoff and J. I. Siepmann, *AIChE Journal* **47**, 1676 (2001)
- 55 P. Virnau, M. Müller, L.G. MacDowell, and K. Binder, *Comp. Phys. Comm.* **147**, 378 (2002)
- 56 P. Virnau, M. Müller, L.G. MacDowell, and K. Binder, *New J. Phys.* **6**, 7 (2004)
- 57 K. Binder, *Phys. Rev. A***25**, 1699 (1982)
- 58 J. E. Hunter III and W. P. Reinhardt, *J. Chem. Phys.* **103**, 8627 (1995)
- 59 J. Potoff and A. Panagiotopoulos, *J. Chem. Phys.* **112**, 6411 (2000)
- 60 R. L. C. Vink and J. Horbach, *J. Phys.: Condens. Matter* **16**, 3807 (2004)
- 61 L. Yelash, P. Virnau, W. Paul, K. Binder, and M. Müller, preprint.
- 62 G. C. Maitland, M. Rigby, E. B. Smith, and W. A. Wakeham, *Intramolecular Forces, Their Origin and Determination* (Clarendon Press, Oxford, 1981)
- 63 K. Binder, M. Müller, P. Virnau, and L. G. MacDowell, *Adv. Polym. Sci.* **1731** (2005)
- 64 M. S. Wertheim, *J. Chem. Phys.* **87**, 7323 (1987)
- 65 L. G. MacDowell, M. Müller, C. Vega and K. Binder, *J. Chem. Phys.* **113**, 419 (2000)
- 66 L. G. MacDowell, P. Virnau, M. Müller, and K. Binder, *J. Chem. Phys.* **117**, 6360 (2002)
- 67 J. P. Hansen, I. R. McDonald, *Theory of Simple Liquids* (Academic, New York, 1986).

- 68 J. A. Barker and D. Henderson, *J. Chem. Phys.* **47**, 4714 (1967)
- 69 Y. Tang and B. C.-Y. Lu, *J. Chem. Phys.* **99**, 9828 (1993)
- 70 Y. Tang, Z. Tong and B. C.-Y. Lu, *Fluid Phase Equilib.* **134**, 21 (1997)
- 71 A. Parola, D. Pini, and L. Reatto *Phys. Rev. Lett.* **100**, 165704 (2008)
- 72 A. Parola, D. Pini, and L. Reatto *Phys. Rev. Lett.* **53**, 2417 (1984)
- 73 W. G. Chapman, K. E. Gubbins, G. Jackson, and M. Radosz, *Fluid Phase Equilib.*, **52**, 31, (1989); L. Yelash, M. Müller, W. Paul, and K. Binder, *Phys. Chem. Chem. Phys.*, **7**, 3728, (2005)
- 74 L. D. Landau and E. M. Lifshitz, *Statistical Physics* (third edition), Butterworth-Heinemann (1996)
- 75 NIST website: <http://webbook.nist.gov/chemistry/>.
- 76 M. W. Pestak, R. E. Goldstein, M. H. W. Chan, J. R. de Bruyn, and N. W. Ashcroft, *Phys. Rev.* **B36**, 599 (1987)
- 77 G. Raabe and R. J. Sadus, *J. Chem. Phys.* **119**, 6691 (2003)
- 78 L. Wang and R. J. Sadus, *J. Chem. Phys.* **125**, 144509 (2006)
- 79 J. C. G. Calado, E. Chang, and W. B. Streett, *Physica* **117A**, 127 (1983)
- 80 P. S. Arora, H. L. Robjohns, and P. J. Dunlop, *Physica A* **95**, 561 (1979).
- 81 M. Klein and H. J. M. Hanley, *J. Chem. Phys.* **53**, 4722 (1970).
- 82 H. J. M. Hanley and M. Klein, *J. Phys. Chem.* **76**, 1743 (1972).
- 83 M. Saharay and S. Balasubramanian, *J. Chem. Phys.* **120**, 9694 (2004)
- 84 Y. Zhang, J. Yang, and Y.-X. Yu, *J. Phys. Chem.* **B109**, 13375 (2005)
- 85 G. Stell, J. C. Rasiaiah, and H. Narang, *Mol. Phys.* **27**, 1392 (1974)
- 86 K. Binder, in *Monte Carlo and Molecular Dynamics Simulations in Polymer Science*, edited by K. Binder (Oxford Univ. Press, New York, 1995), p. 1
- 87 B. Smit, J. L. Siepmann, and S. Karaborni, *J. Chem. Phys.* **102**, 2126 (1995)
- 88 K. Kremer and G. S. Grest, *J. Chem. Phys.* **92**, 5057 (1990)
- 89 K. S. Pitzer, *J. Am. Chem. Soc.* **77**, 3427 (1955)
- 90 L. Zhang and J. I. Siepmann, *J. Phys. Chem.* **B109**, 2911 (2005)
- 91 C. L. Kong, *J. Chem. Phys.* **59**, 2464 (1973)
- 92 B. E. Fender and G. D. Halsey, Jr. *J. Chem. Phys.* **36**, 1881 (1962)
- 93 F. T. Smith, *Phys. Rev.* **A5**, 1708 (1972)

- ⁹⁴ C. Menduiña, C. McBride and C. Vega, PCCP **3**, 1289 (2001)
- ⁹⁵ J. Wang, C. A. Cerdeirina, M. A. Anisimov, and J. V. Sengers, Phys. Rev. E**77**, 031127 (2008)
- ⁹⁶ M. E. Fisher and G. Orkoulas, Phys. Rev. Lett **85**, 696 (2000)
- ⁹⁷ G. Orkoulas, M. E. Fisher, and C. Üstün, J. Chem. Phys. **113**, 7530 (2000)
- ⁹⁸ Y. C. Kim, M. E. Fisher, and G. Orkoulas, Phys. Rev. E**67**, 061506 (2003)
- ⁹⁹ B. H. Sage, W. N. Lacey, and J. G. Schaafsma, Ind. Eng. Chem. **26**, 214 (1934)
- ¹⁰⁰ B. H. Sage, R. H. Olds, and W. N. Lacey, Ind. Eng. Chem. **34**, 1108 (1942)
- ¹⁰¹ T.-C. Chu, R. J. J. Chen, P. S. Chappelaer, and R. Kobayashi, J. Chem. Eng. Data **21**, 41 (1979)
- ¹⁰² H.-M. Lin, H. M. Sebastian, J. J. Simnick, and K.-C. Chao, J. Chem. Eng. Data **24**, 146 (1979)
- ¹⁰³ G. Schneider, Z. Alwani, W. Heim, E. Horvath, and E. U. Franck, Chemie-Ing.-Techn. **39**, 649 (1967)
- ¹⁰⁴ H. Cheng, M. E. P. de Fernandez, J. A. Zollweg, and W. B. Streett J. Chem. Eng. Data **34**, 319 (1989)
- ¹⁰⁵ J. D. Hottovy, K. D. Luks, and J. P. Kohn, J. Chem. Eng. Data **26**, 256 (1981)
- ¹⁰⁶ H. M. Sebastian, J. J. Simnick, H.-M. Lin, and K.-C. Chao, J. Chem. Eng. Data **25**, 138 (1980)
- ¹⁰⁷ B. Garzon, S. Lago, C. Vega, E. de Miguel, and L. F. Rull, J. Chem. Phys. **101**, 4166 (1994)
- ¹⁰⁸ Indeed using results of Ref. 36 the CG parameters for given substances (with a reasonable quadrupolar moment) can be computed in a straightforward way without additional simulations.
- ¹⁰⁹ However sometimes is far from being clear if deviations from LB combining rules are infact compensation of some bias of the model used. For instance in the case of polar substances the present work shows very clearly how strong violations of the rules in Ref. 42 were more properly due to a bad modelling for the solvents.
- ¹¹⁰ It is interesting to observe how atomistic models that are not improved to describe all the pure substances phase diagram but take as experimental input only the critical temperature and density (like in our case) are less accurate than our simpler (see for instance the discussion of EPM2 model⁵¹ in 36).

TABLE I: We report all the simulation parameters used in the present work and the critical parameters of the pure components that have been used. In brackets we also report the errors (if n digits are reported, the error applies to the same last digits). The errors for ϵ and σ have been estimated using the experimental errors for the critical points⁷⁵ and an error of 0.5% in the simulation critical points as estimated previously.³⁶ As a consequence we note for instance that in the three models used for C_6H_6 the three values for σ are almost compatible with our error bar. It is important to observe that in this discussion we have disregarded the huge error in the quadrupolar moment Q (and as a consequence in q). We refer to the text for a discussion of this point.

FIG. 1: (Color online) Illustration of the coarse-graining procedure: in the case of hexadecane, three successive C-C bonds are integrated into one bead (dotted circle). The oligomer, containing 50 atoms (or 16 “united atoms”, CH_3 or CH_2 , respectively) is thus reduced to an effective chain of 5 beads. Neighboring beads along a chain interact with a combination of Lennard Jones (LJ) and finitely extensible nonlinear elastic (FENE) potentials. Non-bonded beads only interact with a single LJ potential. Carbon dioxide is represented by a point particle, which carries a quadrupole moment.

FIG. 2: (Color online) Coexistence curve for Kr (upper curve) and Xe (lower curve) in the temperature density-plane (a), and interface tension plotted vs. temperature (b). Broken curves indicate the experimental data,⁷⁵ asterisks MC results where ρ_c^{exp} was used to adjust σ , while circles show data where p_c^{exp} was used to adjust σ (cf. text).

FIG. 3: (Color online) Coexistence pressures for pure Krypton (right) and Xenon (left) plotted vs. temperature. The broken line shows the experimental data for the pure noble gases, while the full curve is the projection of the critical line of the binary mixture (to be discussed in Sec. III.A).⁷⁸ The symbols denote our simulation data (the notation is the same as in fig. 2).

FIG. 4: (Color online) Coexistence curve for CH₄ in the temperature-density plane (a), vapor pressure at coexistence (b) and surface tension plotted vs. temperature (c). Broken curves show experimental data (Ref. 75), crosses the Monte Carlo simulation results, while the full lines show the MSA predictions.

FIG. 5: (Color online) Coexistence curve describing vapor-liquid equilibrium for benzene (C₆H₆) in the temperature density plane (a), temperature dependence of the vapor pressure (b) and the interfacial tensions (c) at phase coexistence. The full curve is the result of fitting T_c^{exp} , ρ_c^{exp} ⁷⁵ to a simple LJ model without taking into account any contribution from quadrupolar interactions, while triangles are Monte Carlo results using Eq. (9) and crosses Eq. (11), respectively. Broken curves are the experimental data.⁷⁵

FIG. 6: (Color online) Coexistence densities for the alkanes studied in the present paper. The following substances are reported (from below): Methane (CH₄), Propane (C₃H₈), Pentane (C₅H₁₂) and Hexadecane (C₁₆H₃₄). Curves are experimental data,⁷⁵ while the open circles are our simulation results.

FIG. 7: (Color online) Coexistence pressures plotted vs. temperature, for the alkanes studied in the present paper, namely CH₄, C₃H₈, C₅H₁₂ and C₁₆H₃₄ (from left to right). Curves are experimental data,⁷⁵ dots show our simulation results.

FIG. 8: (Color online) Interface tensions plotted vs. temperature, for the alkanes studied in the present paper, namely CH₄, C₃H₈, C₅H₁₂ and C₁₆H₃₄ (from left to right). Curves are experimental data,⁷⁵ dots show our simulation results.

FIG. 9: (Color online) (a) Krypton concentration at criticality plotted vs. temperature; the curve shows the experimental data,⁷⁹ while symbols denote our simulation data (the notation is the same as in fig. 2).

FIG. 10: (Color online) Isothermal slice through the phase diagram of the mixture of CH_4 and C_3H_8 at $T = 327\text{K}$ (a) and $T = 277\text{K}$ (b), using the molar fraction x of CH_4 as abscissa variable and pressure p as the ordinate variable. Dots are experimental data⁹⁹ broken curves result from our TPT1-MSA approximation, and symbols denote Monte Carlo data (see text). Triangles are MC results for the critical points.

FIG. 11: (Color online) Isothermal slice through the phase diagram of the mixture of CH_4 and C_5H_{12} at $T = 378\text{K}$ (a) and $T = 237\text{K}$ (b). Triangles denote experimental data,^{100,101} broken curve denotes TPT1-MSA, and asterisks denote Monte Carlo results (which were only taken for $T = 378\text{K}$). Triangles are MC results for the critical points.

FIG. 12: (Color online) Isothermal slices through the phase diagram of the $\text{CH}_4 + \text{CO}_2$ system at $T = 270\text{K}$ (a), $T = 250\text{K}$ (b) and $T = 230\text{K}$ (c). Dots represent experimental data⁹⁹ while the broken curves are the results of TPT1-MSA when CO_2 is represented as a point particle with no quadrupole moment ($q_c = 0$). The full curves are results of TPT1-MSA with the spherically averaged quadrupolar interaction using the parameters of Eq. (8) ($q_c = 0.387$). The triangle shows the MC result for the critical point.

FIG. 13: (Color online) Isothermal slices through the phase diagram of the $\text{CH}_4 + \text{C}_6\text{H}_6$ systems at $T = 501.15\text{K}$ (a), $T = 461.85\text{K}$ (b) and $T = 421.05\text{K}$ (c). Full dots show experimental data¹⁰² curves are calculations based on TPT1-MSA: broken curves denote the simple LJ model ($q_c = 0$), dash-dotted curves are based on Eq. (9), and full curves on Eq. (11). The triangle shows the MC result for the critical point.

FIG. 14: (Color online) Isothermal slice through the phase diagram of the $\text{CO}_2 + \text{C}_5\text{H}_{12}$ system at $T = 423.48\text{K}$ (a) and $T = 344.34\text{K}$ (b). Full dots represent experimental data,¹⁰⁴ asterisks our Monte Carlo results for the model, Eq. (10), while the full curve is the corresponding TPT1-MSA prediction. The broken curve shows the corresponding TPT1-MSA result for a CO_2 model with no quadrupole moment ($q_c = 0$). Triangles are MC results for the critical points.

FIG. 15: (Color online) Isothermal slice through the phase diagram of the $\text{CO}_2 + \text{C}_{16}\text{H}_{34}$ system at $T = 486\text{K}$, showing MC results for the present model (open circles) and comparing them to the results of the previous simulations⁴² with $q_c = 0, \xi = 1$ (full dots) and $q_c = 0, \xi = 0.886$ (asterisks). Squares show two sets of experimental data¹⁰⁶ at two temperatures that bracket the temperature used in the simulation. Triangles are MC results for the critical point.

FIG. 16: (Color online) Critical line of the $\text{CO}_2 + \text{C}_{16}\text{H}_{34}$ mixture, projected onto the p^*, T^* plane (pressure p and temperature T are rescaled with the LJ parameters of the effective monomers of hexadecane as usual, $p^* = p\epsilon/\sigma^3$ and $T^* = k_B T/\epsilon$). Different symbols (as indicated in the figure) denote data with $q_c = 0, \xi = 0.886$ (top curve) and $\xi = 0.9, \xi = 1$ (lowest curve), as well as data for nonzero quadrupole moment, $q_c = 0.387$ and $q = 0.47$, respectively.

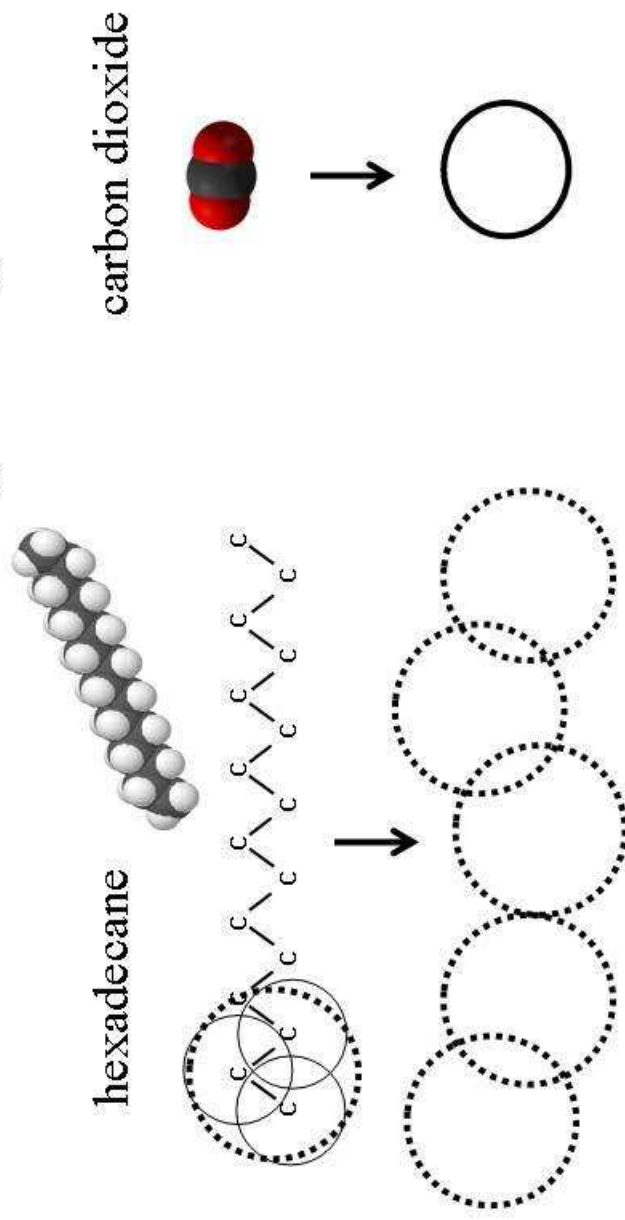
FIG. 17: (Color online) Final normalized order parameter histogram $P(M)$ of Xenon-Krypton mixtures (curve) at $T_1 = 228.78$. The simulated (s) and reweighted (r) parameters (in units of ϵ_x and σ_x) are $\mu_{Ks}^* = -2.254$, $\mu_{Kr}^* = -2.2512$, $\mu_{xs}^* = -3.972$, $\mu_{xr}^* = -3.9792$, $x_1 = 0.4$, $x_2 = 0.03$. The dots show the universal 3d Ising model distribution.

FIG. 18: (Color online) (a) Plot of B_4 and B_2 as a function of μ_s for the $\text{CO}_2 + \text{C}_{16}\text{H}_{34}$ mixture ($T=1.16$). The chemical potential μ_p was always chosen such that the equal weight rule was obeyed. Three different box linear dimensions are included, as indicated. The broken horizontal lines indicate the universal values B_4^* and B_2^* of the Ising model at criticality, where the intersections of the curves for B_4 and B_2 in the finite size scaling limit ($L \rightarrow \infty$) should occur. These data have been generated for the mixing parameter $x_1 = 0.09$. The inset shows a plot of B_4 vs. x_1 for $L = 13.5\sigma_p$ for three different values of μ_s . (b) Probability distribution $P(n_p, n_s)$ of the numbers of polymers (n_p) and solvent molecules (n_s) for $L = 13.5\sigma_p$ at criticality.

	q_c	$\epsilon/10^{-21}\text{J}$	$\sigma/\text{\AA}$	T_c/K	$\rho_c/(\text{mol/l})$	p_c/bar	$p_{c,\text{sim}}/\text{bar}$
Kr	0	2.8971(145)	3.6524(126)	209.46(2)	11.0(1)	55.20(6)	52.33(66)
	0	2.8971(145)	3.58782(2568)	209.46(2)	11.0(1)	55.20(6)	55.2(1.2)
Xe	0	4.00747(2004)	4.00053(685)	289.74(2)	8.37(1)	58.42(6)	55.08(48)
	0	4.00747(2004)	3.92326(2803)	289.74(2)	8.37(1)	58.42(6)	58.4(1.3)
CO ₂	0	4.20648(2104)	3.69489(627)	304.13(4)	10.62(5)	73.77(15)	73.30(64)
	0.387	3.49047(1746)	3.78467(641)	304.13(4)	10.62(5)	73.77(15)	73.10(64)
	0.47	3.34887(1675)	3.80341(645)	304.13(4)	10.62(5)	73.77(15)	73.10(64)
C ₆ H ₆	0	7.77317(4041)	5.16046(8863)	562.0(8)	3.9(2)	48.9(4)	49.7(2.6)
	0.247	6.90972(3592)	5.24125(9002)	562.0(8)	3.9(2)	48.9(4)	49.5(2.6)
	0.382	6.47249(3365)	5.28363(9075)	562.0(8)	3.9(2)	48.9(4)	49.5(2.6)
CH ₄	0	2.63624(1382)	3.75782(2558)	190.6(3)	10.1(2)	46.1(3)	43.70(95)
C ₃ H ₈	0	5.11618(2573)	4.71826(12360)	369.9(2)	5.1(4)	42.5(1)	42.5(3.4)
C ₅ H ₁₂	0	4.86594(2487)	4.30303(3200)	469.8(5)	3.22(7)	33.6(6)	31.90(75)
C ₁₆ H ₃₄	0	5.78879(4320)	4.57052(4787)	722(4)	0.967(30)	14(2)	12.80(42)

TABLE 1

Coarse graining



Bead-spring model : LJ+FENE potential

FIG. 1

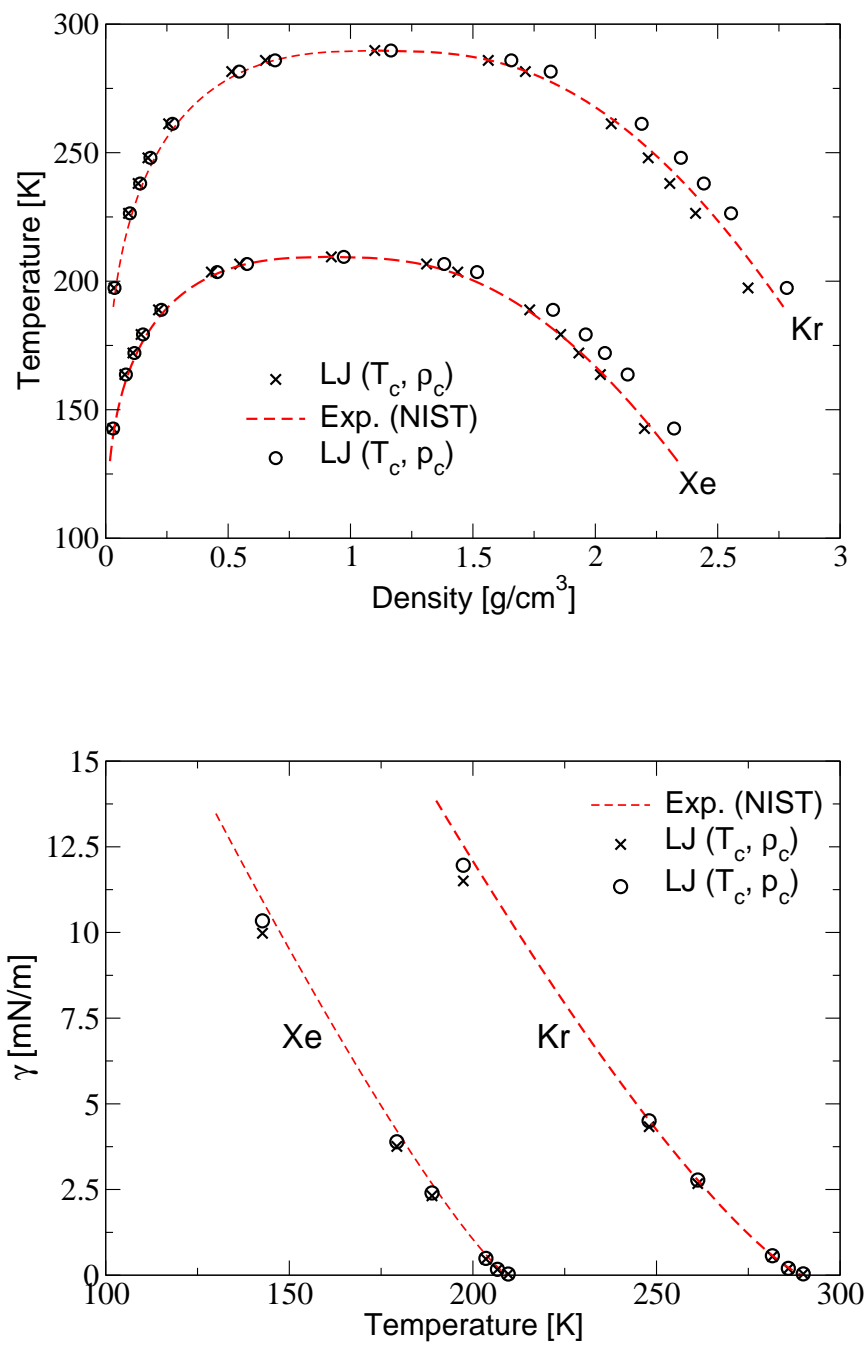
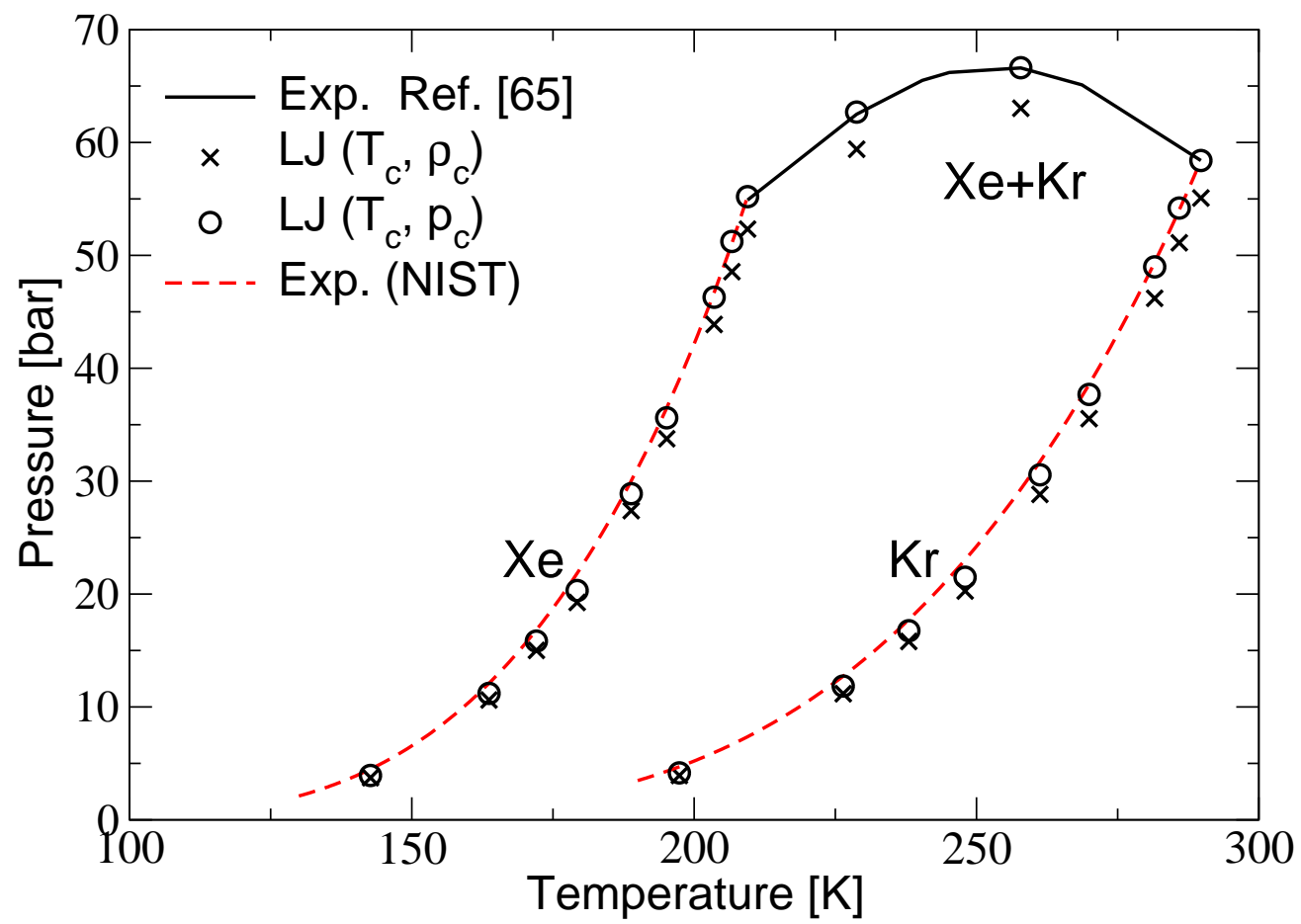


FIG. 2

FIG. 3



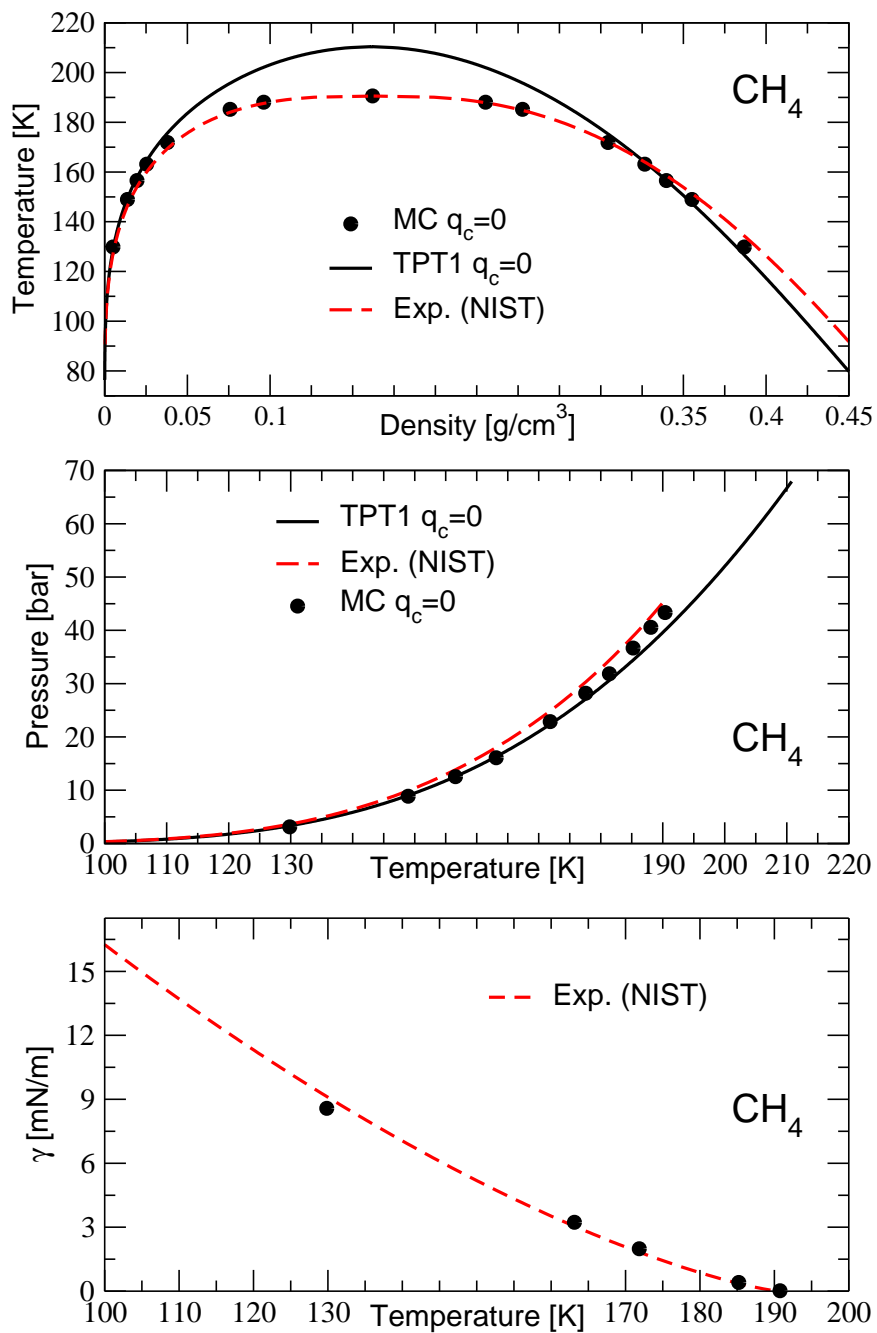


FIG. 4

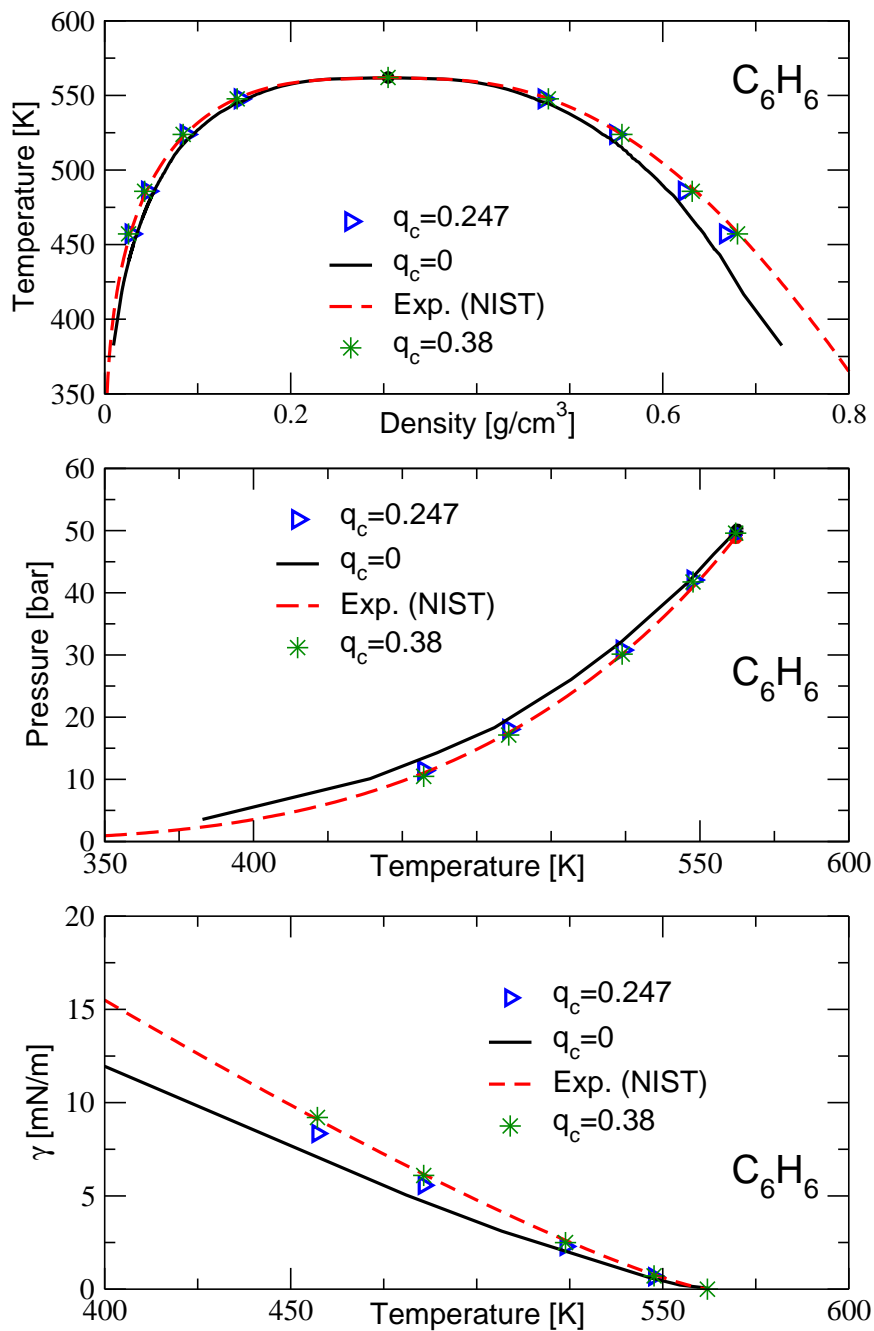
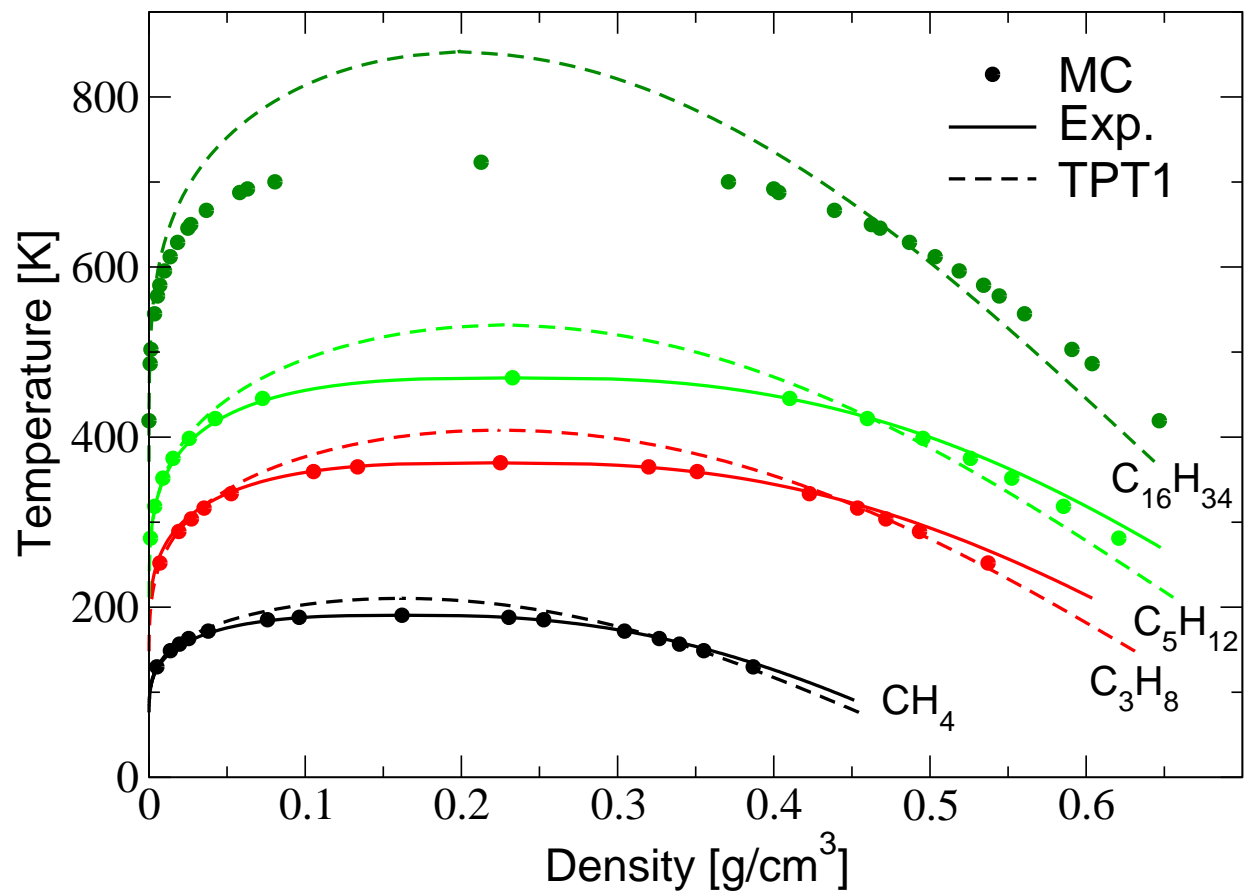


FIG. 5

FIG. 6



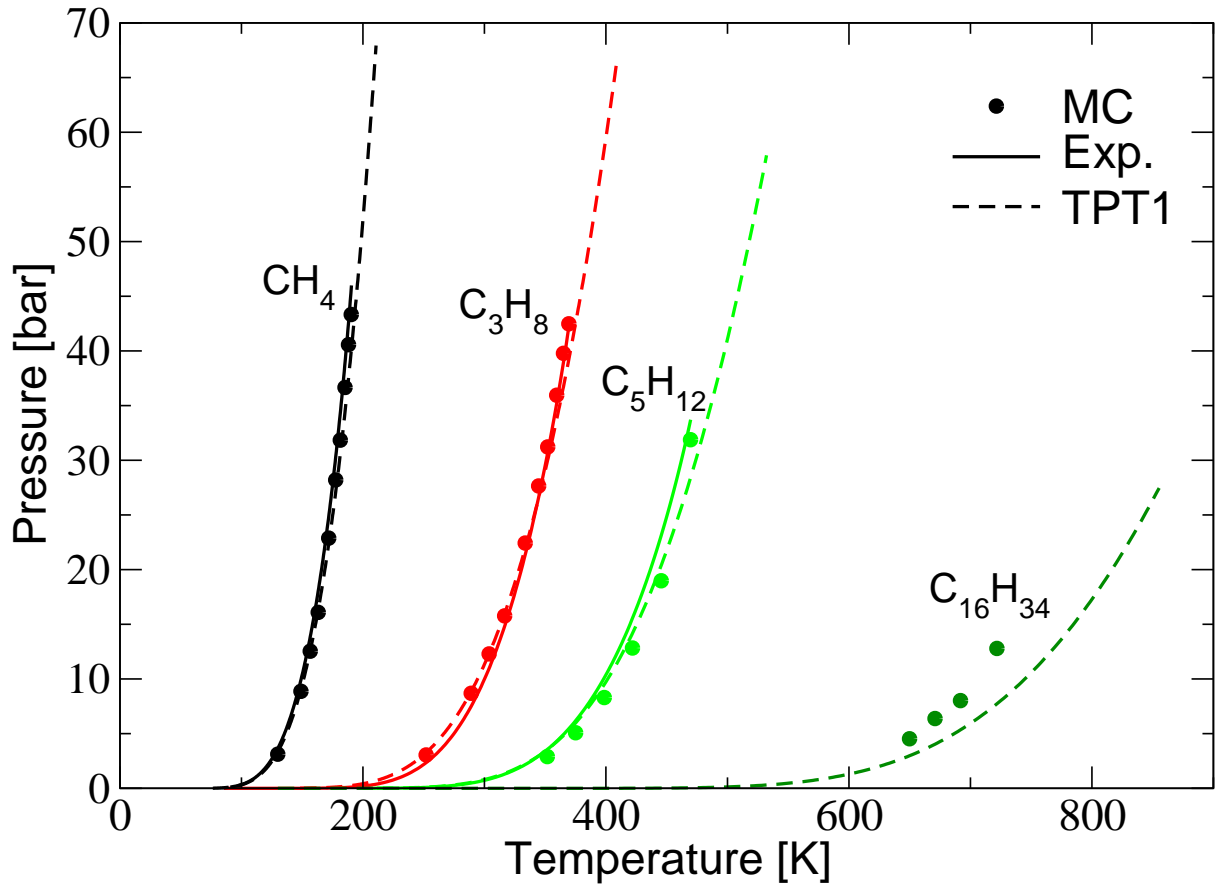


FIG. 7

FIG. 8

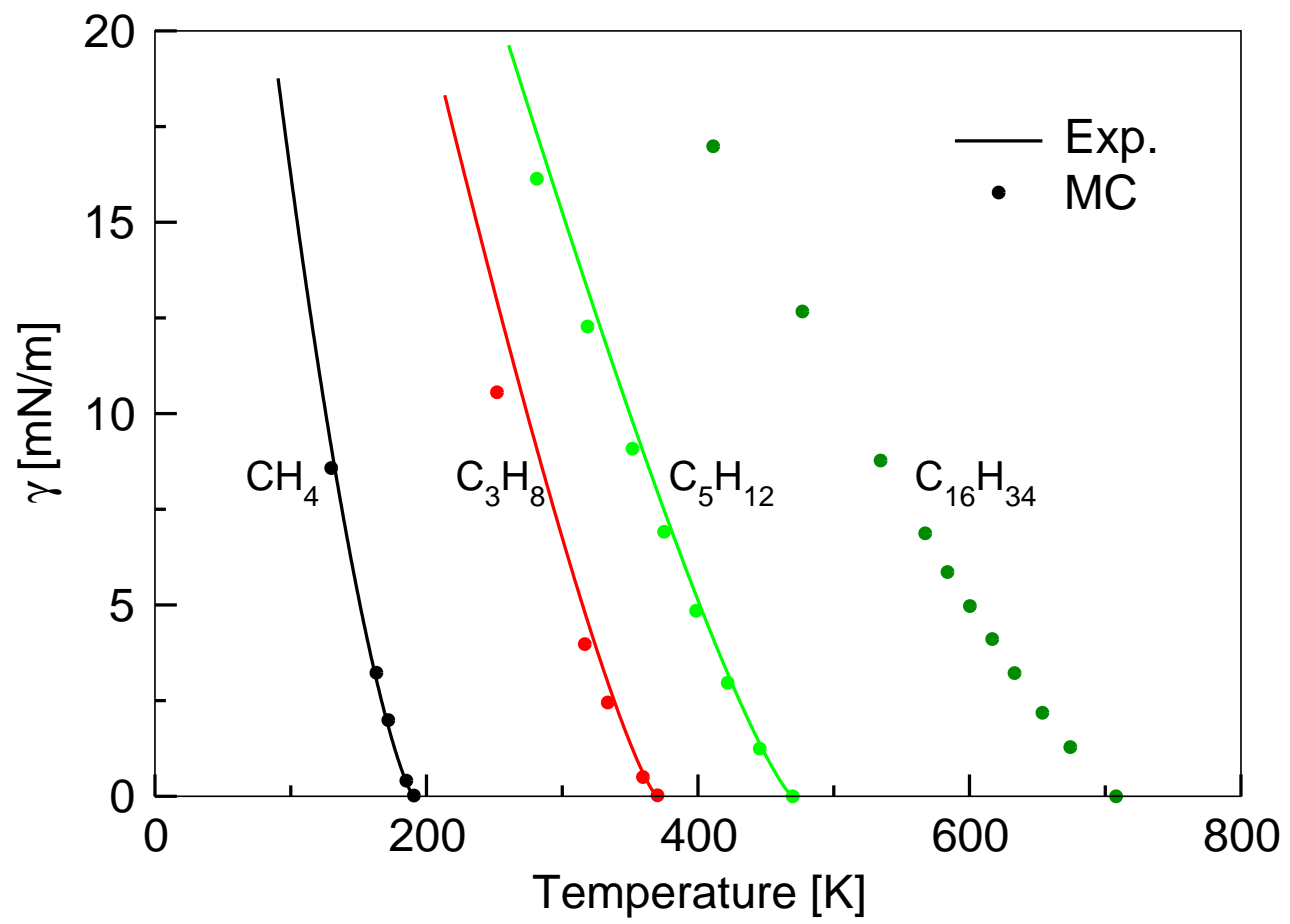
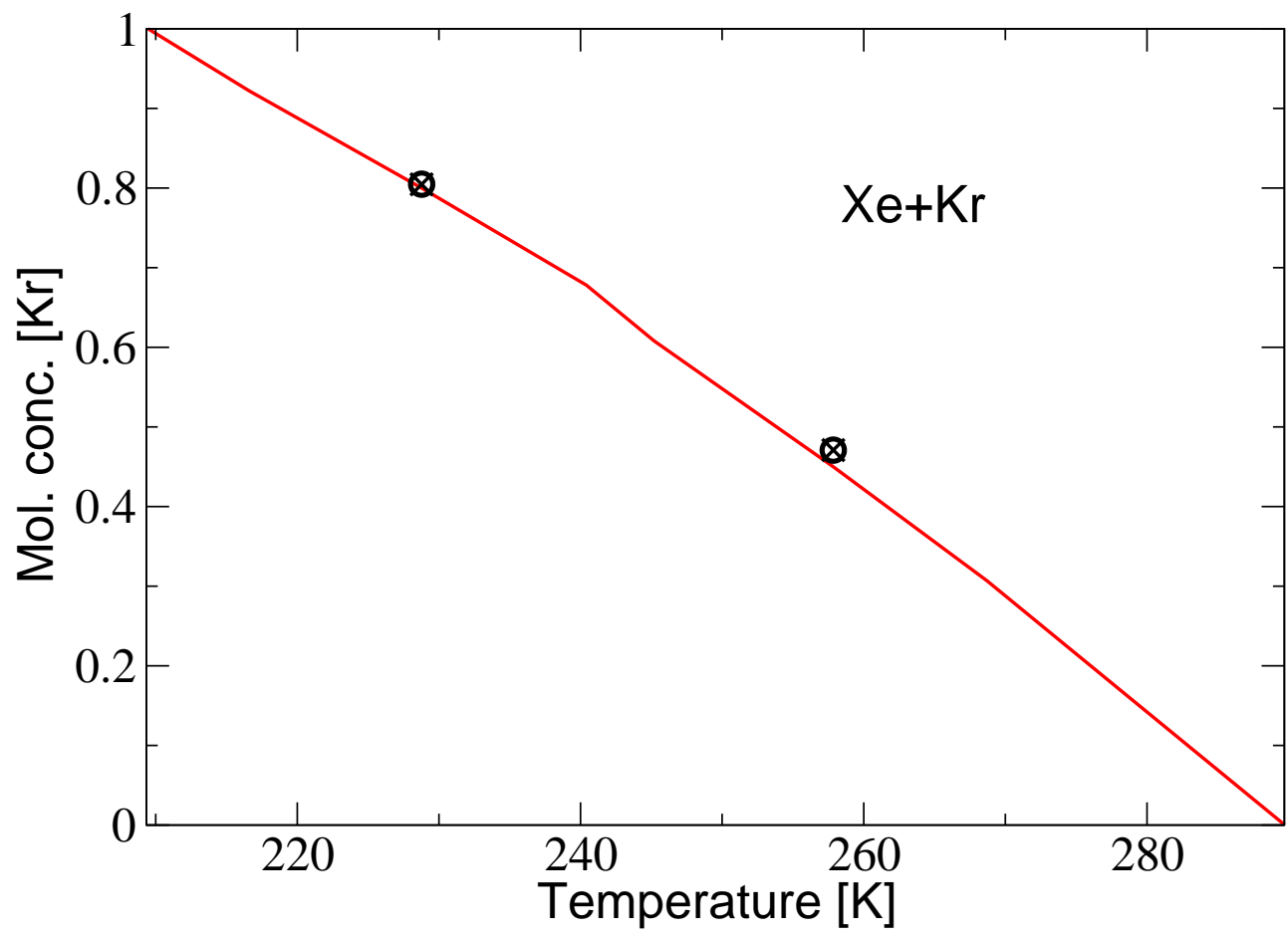


FIG. 9



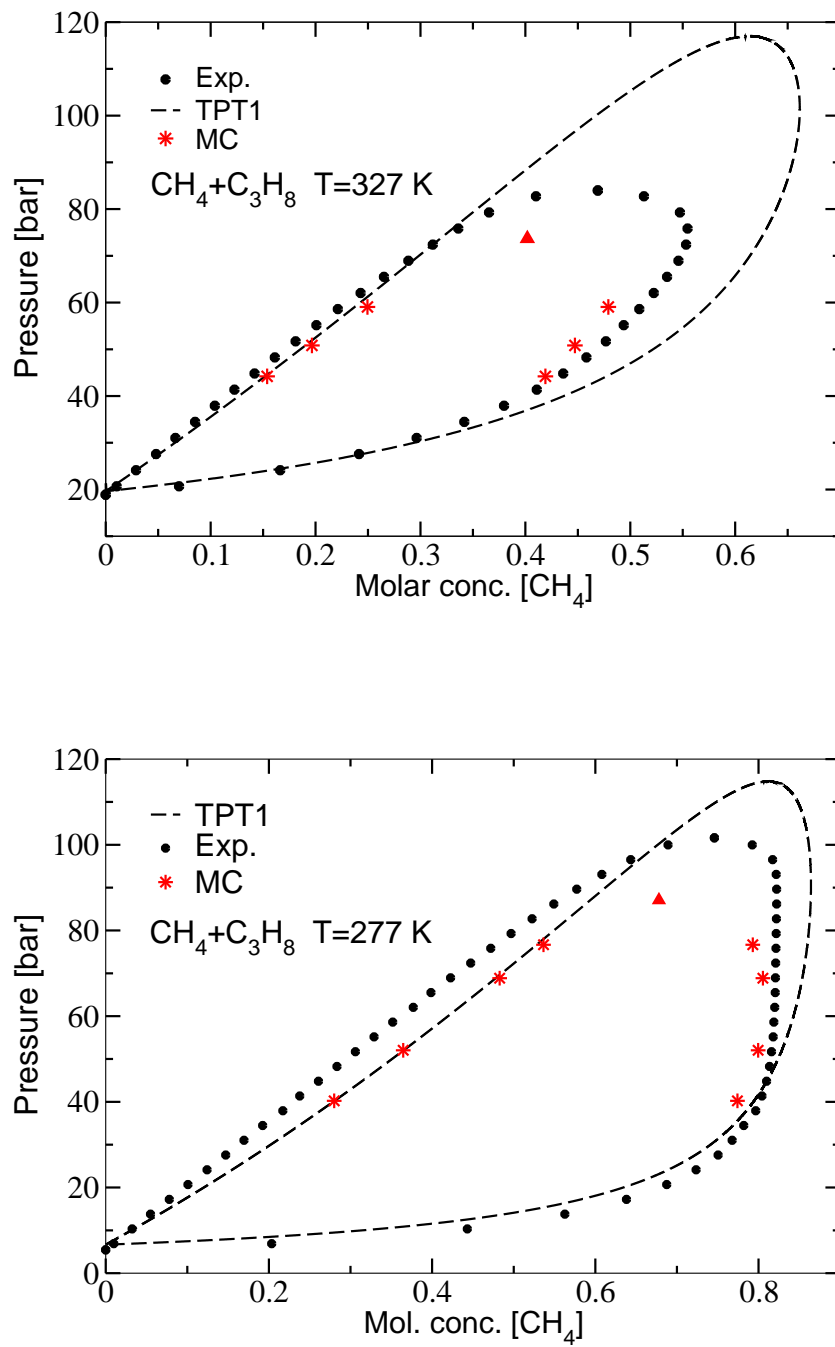


FIG. 10

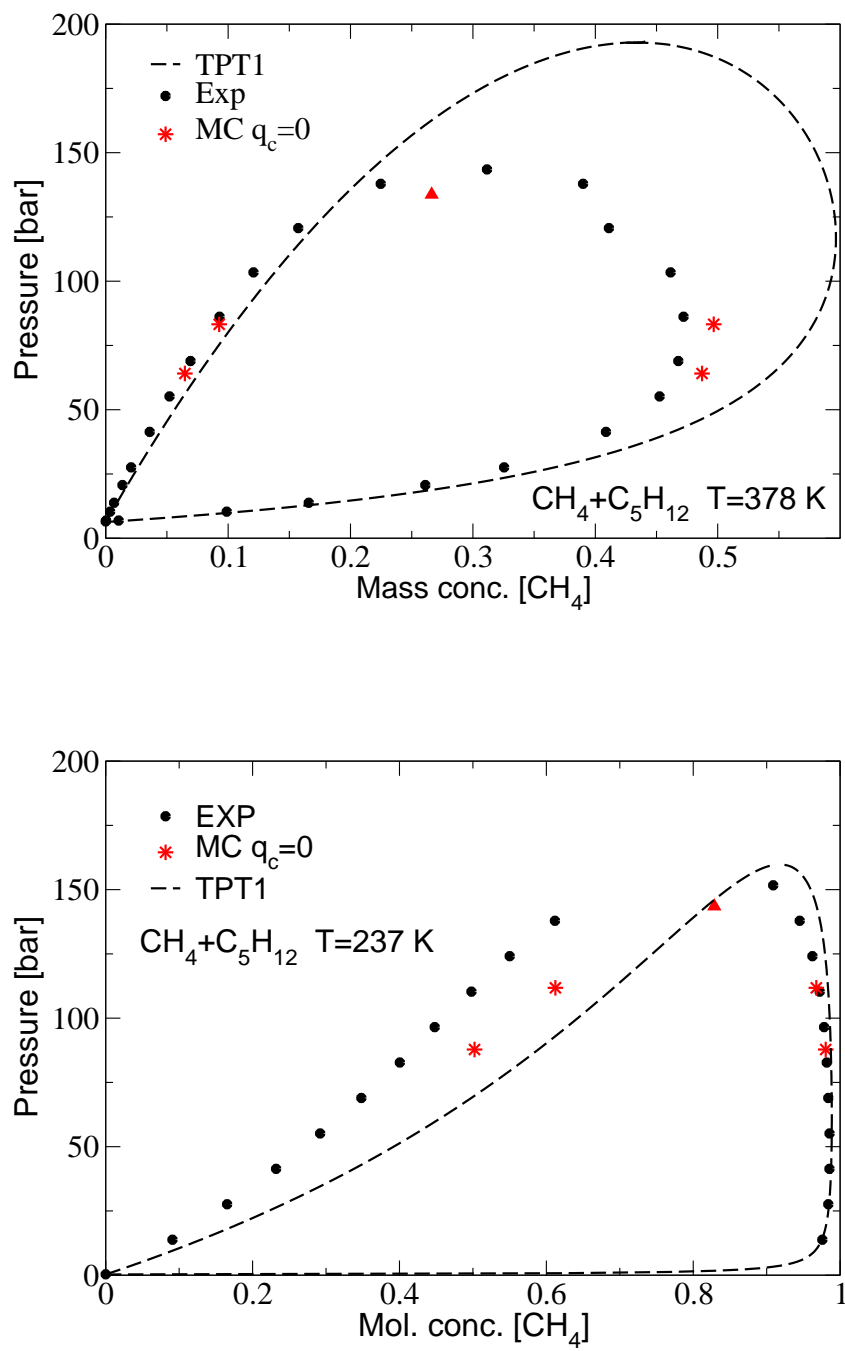


FIG. 11

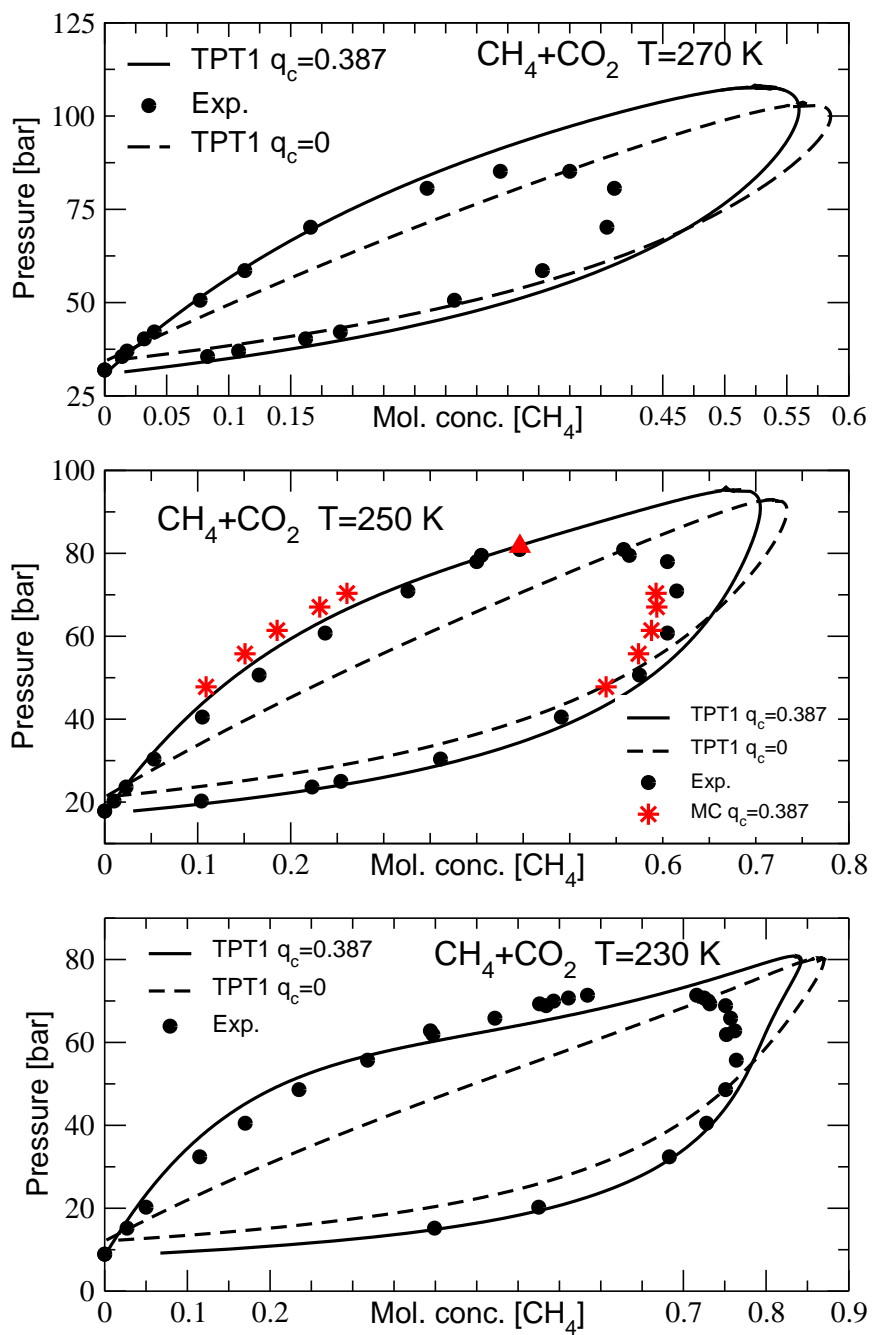


FIG. 12

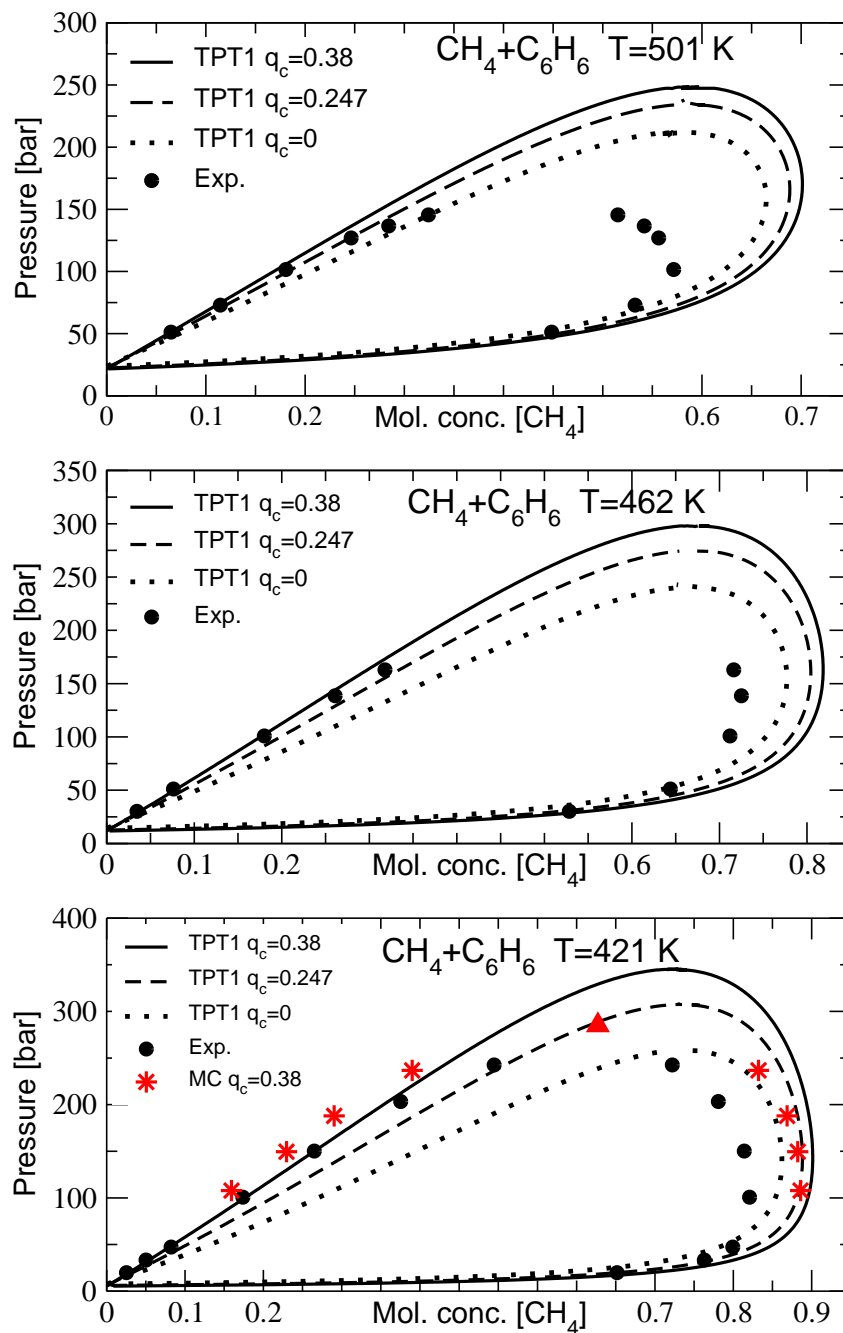


FIG. 13

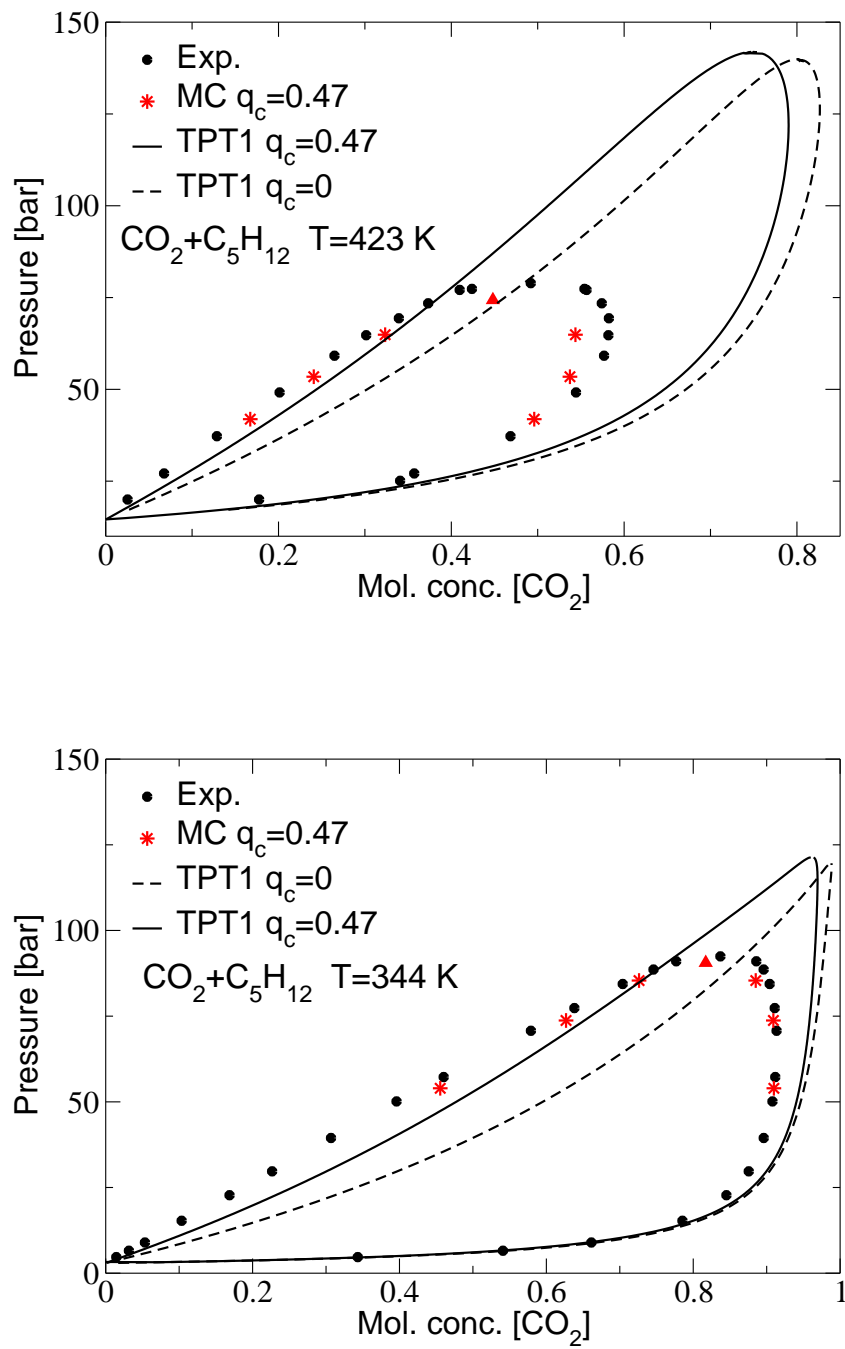


FIG. 14

FIG. 15

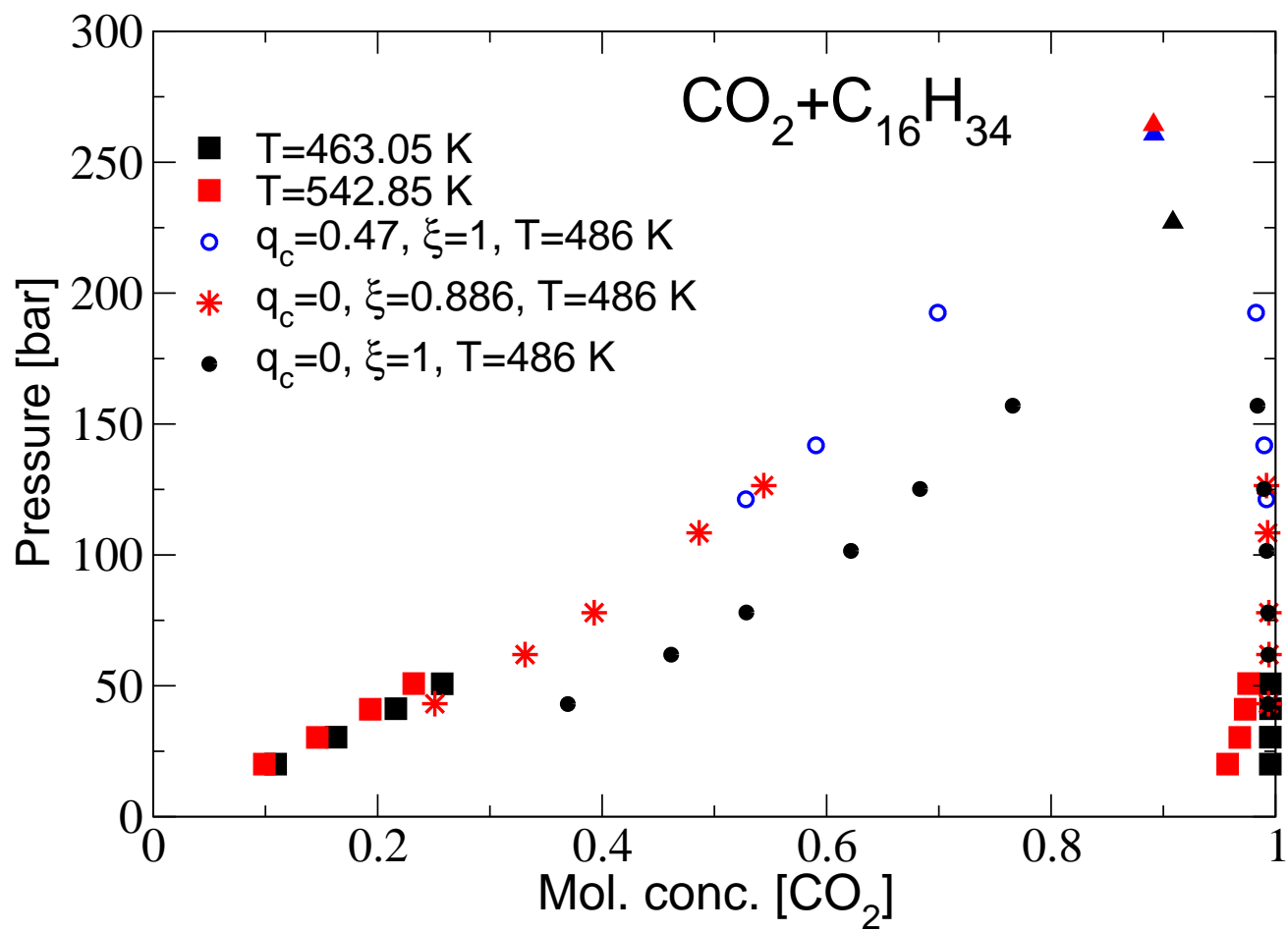
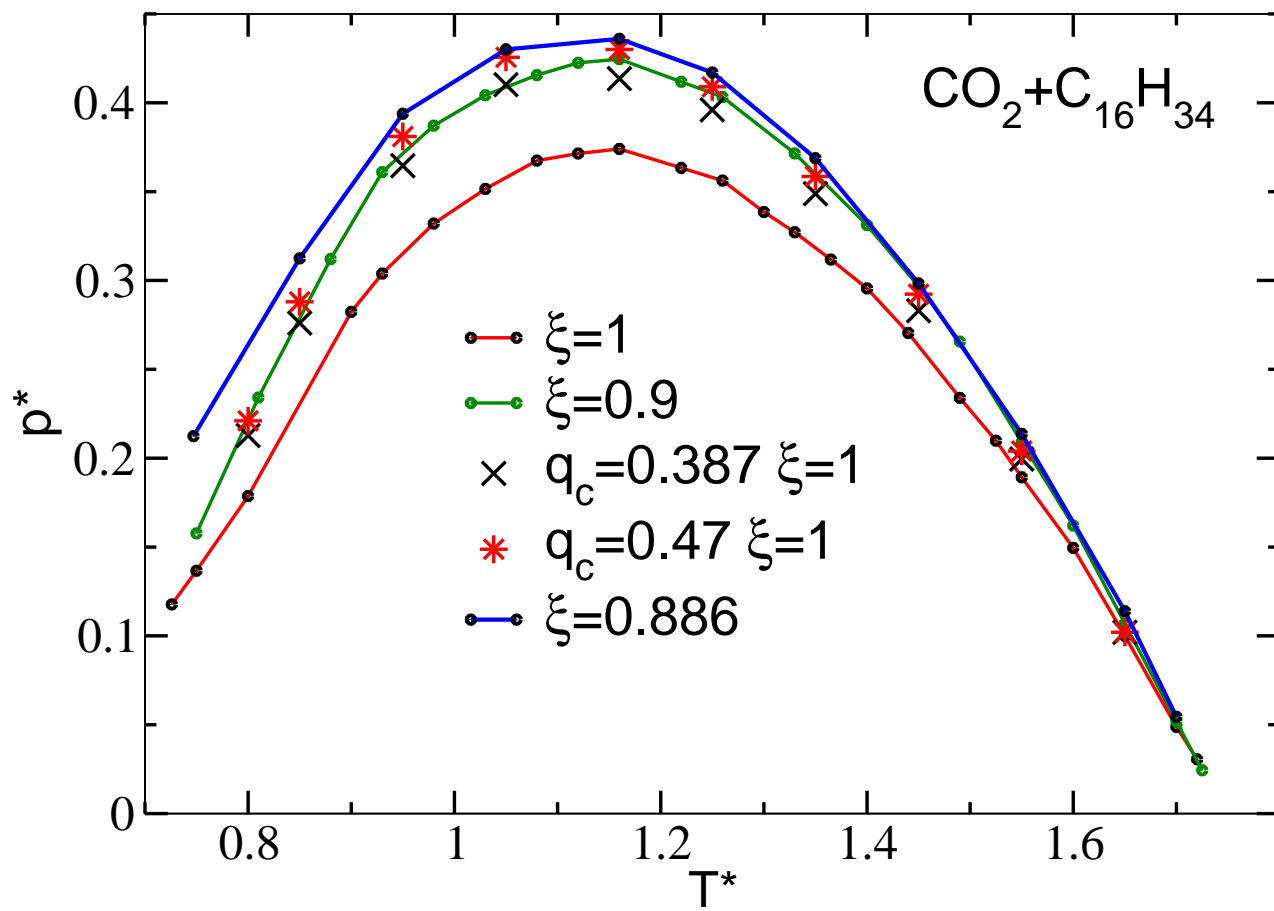


FIG. 16



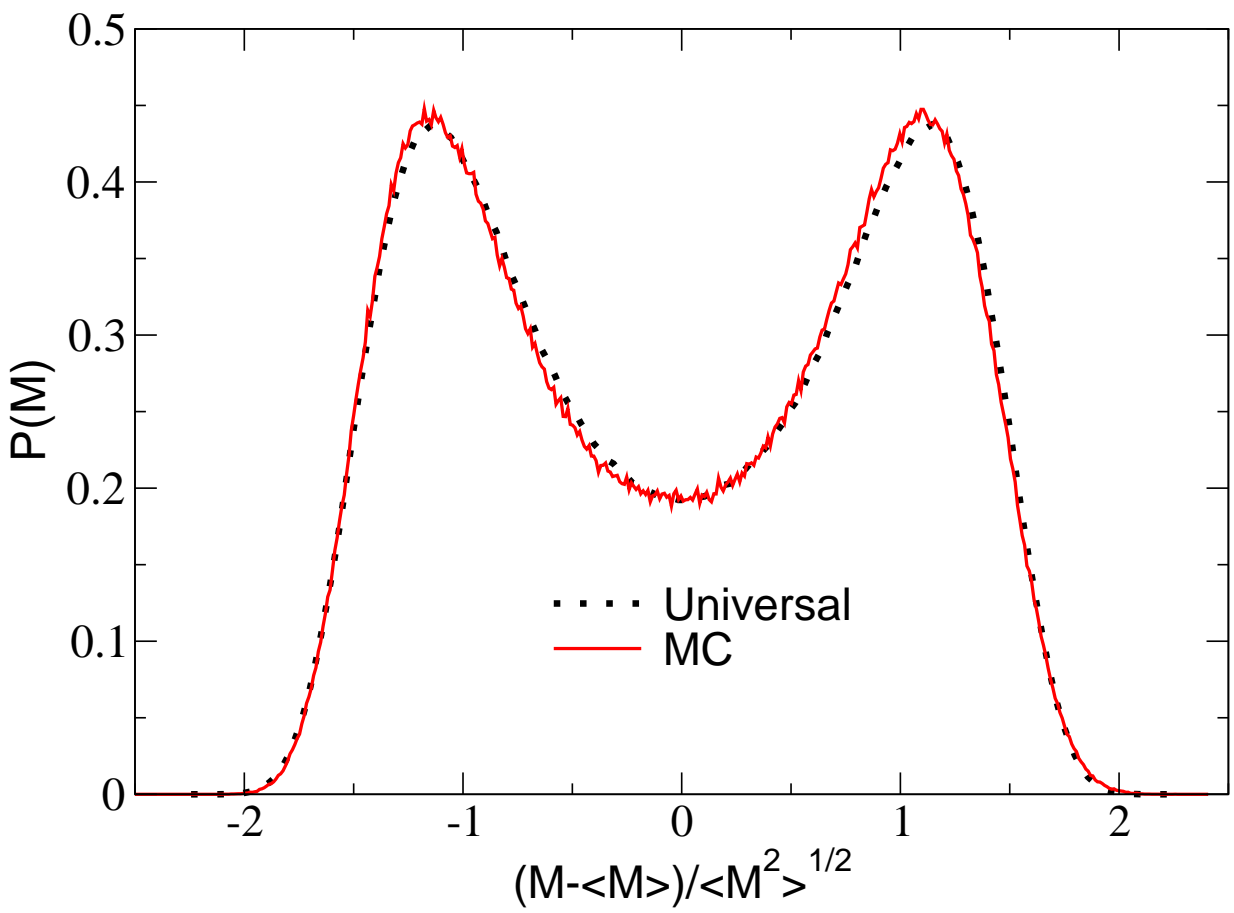


FIG. 17

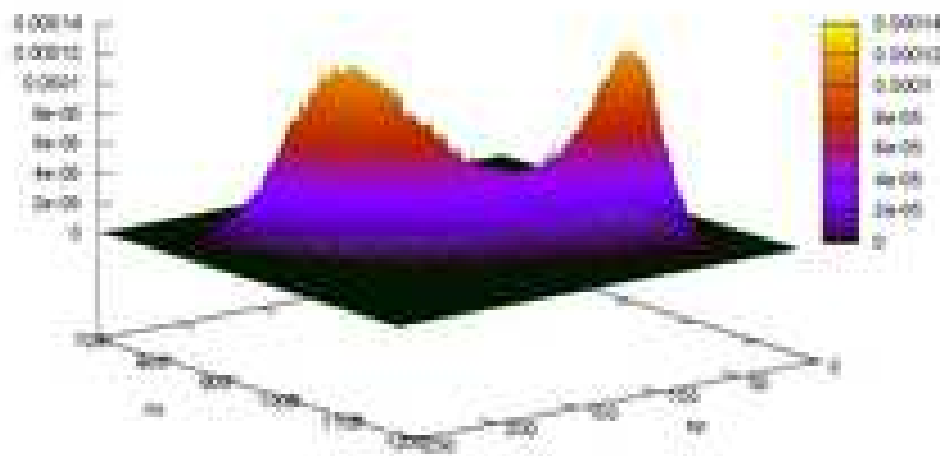
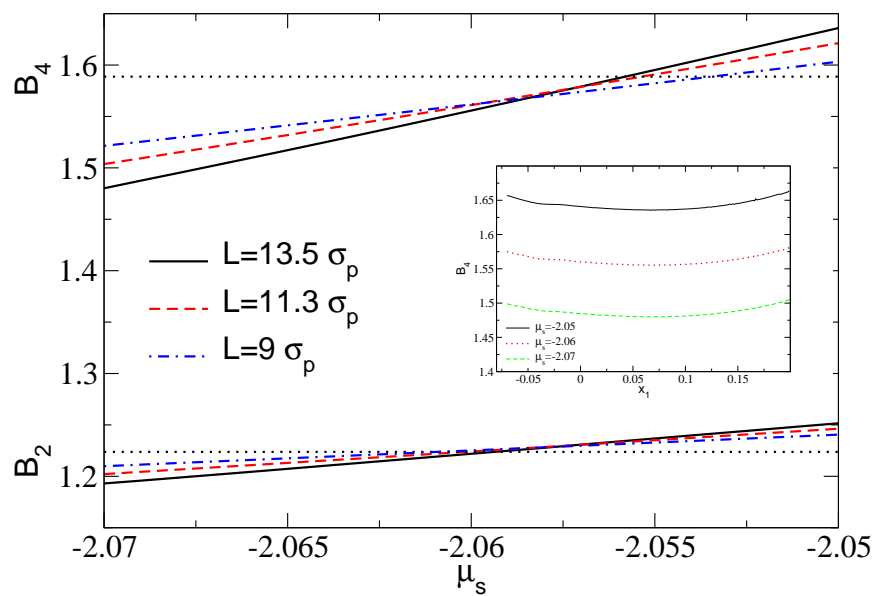


FIG. 18